ON THE COMPLEXITY OF SHAPES EMBEDDED IN $\mathbb{Z}^n$

A THESIS SUBMITTED TO
THE GRADUATE SCHOOL OF NATURAL AND APPLIED SCIENCES
OF
MIDDLE EAST TECHNICAL UNIVERSITY

BY

MAZLUM FERHAT ARSLAN

IN PARTIAL FULFILLMENT OF THE REQUIREMENTS
FOR
THE DEGREE OF MASTER OF SCIENCE
IN
COMPUTER ENGINEERING

SEPTEMBER 2019

Approval of the thesis:

ON THE COMPLEXITY OF SHAPES EMBEDDED IN $\mathbb{Z}^n$

submitted by **MAZLUM FERHAT ARSLAN** in partial fulfillment of the requirements for the degree of **Master of Science in Computer Engineering Department, Middle East Technical University** by,

Prof. Dr. Halil Kalıpçılar
Dean, Graduate School of **Natural and Applied Sciences** _____

Prof. Dr. Halit Oğuztüzün
Head of Department, **Computer Engineering** _____

Prof. Dr. Sibel Tarı
Supervisor, **Computer Engineering, METU** _____

Examining Committee Members:

Prof. Dr. Tolga Kurtuluş Çapın
Computer Engineering, TED University _____

Prof. Dr. Sibel Tarı
Computer Engineering, METU _____

Prof. Dr. Pınar Karagöz
Computer Engineering, METU _____

Date:

I hereby declare that all information in this document has been obtained and presented in accordance with academic rules and ethical conduct. I also declare that, as required by these rules and conduct, I have fully cited and referenced all material and results that are not original to this work.

Name, Surname: Mazlum Ferhat Arslan

Signature :

ABSTRACT

ON THE COMPLEXITY OF SHAPES EMBEDDED IN $\mathbb{Z}^N$

Arslan, Mazlum Ferhat
M.S., Department of Computer Engineering
Supervisor: Prof. Dr. Sibel Tarı

September 2019, 71 pages

Shape complexity is a hard-to-quantify quality, mainly due to its relative nature. In common view, circles are considered to be the simplest shapes. However, when implemented in computer, none of the circularity measures yield the expected scores for the circle. This is because digital domain ($\mathbb{Z}^n$) realizations of circles are only approximations to the ideal form. Consequently, complexity orders computed in reference to circle are unstable. As a remedy, we consider squares to be the simplest shapes relative to which multi-scale complexity orders are to be constructed. Whereas measuring roundness is encountered more often in literature quantifying rectangularity emerges as a specific interest due to applications ranging from landscape ecology, urban planning, and computer-aided production. Using the connection between L^∞ and squares we effectively encode squareness-adapted multi-scale simplification through which we obtain entropy-like multi-scale shape complexity measure. In contrast to usual diffusion based ones, our multi-scale simplification exhibits a local behavior where curves become locally flat instead of getting rounder. Proposed complexity measure is tested on binary images containing noisy shapes; Kendall-τ distances from the expected order are reported. The measure is compared against its L^2 counterpart in

terms of robustness under noise and scale. Finally, partial orders are constructed on the shapes based on their complexities with respect to different scales and various complexity measures.

Keywords: Shape Complexity, Information Theory, Infinity Laplacian, Squareness, Rectangularity, Partial Order, Level Set-Based Analysis

ÖZ

$\mathbb{Z}^N$'DE GÖMÜLÜ ŞEKİLLERİN KARMAŞIKLIĞI ÜZERİNE

Arslan, Mazlum Ferhat
Yüksek Lisans, Bilgisayar Mühendisliği Bölümü
Tez Yöneticisi: Prof. Dr. Sibel Tarı

Eylül 2019, 71 sayfa

Şekil karmaşıklığı göreceli doğasından ötürü nicelendirilmesi zor olan bir niteliktir. Genel görüşün en basit şekillerin daireler olduğu yönünde olmasına karşın dairesellik ölçen yöntemler bilgisayar temelli uygulanmalarında daireler için ideal sonuçları vermemektedir. Bunun sebebi dairelerin dijital ortamda ($\mathbb{Z}^n$), ideal formlarının yaklaşık gerçekleştirilmeleri olarak zuhur etmesidir. Dolayısıyla daireler temel alınarak yapılan karmaşıklık sıralamaları istikrarsızdır. Çözüm olarak kareleri en basit şekiller olarak ele alıyor ve bu temelde çoklu ölçekli karmaşıklık ölçümleri oluşturuyoruz. Literatürde dairesellik ölçümleriyle daha sık karşılaşılmasına karşın dikdörtgensellik ölçümleri de peyzaj ekolojisi, şehir planlama ve bilgisayar destekli üretim gibi uygulamalar dolayısıyla öne çıkmaktadır. L^∞ uzayı ve kareler arasındaki bağlantıdan yararlanarak karelik temelli çoklu ölçekli basitleştirmeler kodluyor ve bunlardan entropi benzeri çoklu ölçekli şekil karmaşıklığı ölçümleri elde ediyoruz. Sıklıkla kullanılan yayılım temelli basitleştirmede görülen şekil kıvrımlarının yuvarlaklaşması davranışının aksine, önerdiğimiz basitleştirmede kıvrımlar yerel olarak düzleşmektedir. Önerilen karmaşıklık ölçümü istatistiksel olarak oluşturulmuş gürültülü siyah beyaz şekiller üzerinde test edilmiş ve beklenen sıralamalara olan Kendall-τ mesa-

feleri raporlanmıştır. Ölçüm, L^2 karşılığı ile gürültü ve ölçek altındaki değişimler karşısındaki sağlamlıkları bakımından karşılaştırılmıştır. Son olarak, önerilen yöntemin farklı ölçeklerdeki uygulamaları ve farklı karmaşıklık sıralamaları kullanılarak şekiller üzerinde kısmi sıralamalar oluşturulmuştur.

Anahtar Kelimeler: Şekil Karmaşıklığı, Bilgi Kuramı, L^∞ Laplasyen, Karelik, Dikdörtgenlik, Kısmi Sıralama, Eşdüzey Eğrileri Temelli Analiz

To the eye that seeks what it is missing

ACKNOWLEDGMENTS

I thank my advisor Prof. Sibel Tari for the guided freedom she provided while doing this research, the inspiring talks in A403, and her understanding.

I thank my beloved girlfriend Özge Çomak for her ever-present cheerfulness and emotional support.

Lastly, I would like to thank to my parents, Kübra and Hasan Arslan, for their support and guidance throughout my life.

TABLE OF CONTENTS

LIST OF TABLES

TABLES

LIST OF FIGURES

FIGURES

CHAPTER 1

INTRODUCTION

By complexity of an object we mean how easy it is to describe its certain aspects in terms of certain tools. If the object is some data that is to be transmitted digitally, we may consider Shannon entropy [1] -or some variant of it, such as LMC complexity [2]-, or if the data is to be specified, we may consider Kolmogorov complexity [3] as the complexity of the data. If the object is a dynamical system, representability of patterns of trajectories in the phase space can be considered as an indicator of the complexity of the system. Examples can be enriched. The gist is, for a given object, the complexity has to do with how it is of interest (*i.e.* transmitting the data, or specifying it), and what tools are available to describe it (*i.e.* it is easier to construct a circle if compasses are available, or a triangle if rulers are available). Therefore, complexity is relative and not well-defined.

1.1 Shape Complexity

In our take on the shape complexity, shapes are considered by *how constructible they are by a digital computer*. In the scope of this thesis, the word shape is used to refer to compact subsets of two or more dimensional integer spaces with proper grid cell topology, i.e. eight connected in two dimensions, twenty-six connected in three dimensions etc. In the literature other definitions of shapes and other considerations of shape complexity exist as can be inferred from the brief overview presented below.

Earliest interests in shape complexity can be traced back to the *isoperimetric problem* which is the problem of finding which contour, among those of equal perimeters, encloses the maximal area. Note that this is a geometrical consideration of complexity

of shapes. From this problem follows the form factor, a measure given by $4\pi A/P^2$ for a two dimensional shape of perimeter P and area A, and is maximized for circles. The form factor and its variants that manipulate the original arithmetically are reviewed by Ritter and Cooper [4]. For a comprehensive account of the isoperimetric problem, the reader is referred to [5].

An early modern work on shape complexity is the seminal work of Attneave [6]. There, it is demonstrated that complexity appeared to be determined by symmetry, the number of turns and differences in degrees between successive turns in the contour (shape boundary). Results further supporting the effect of number of turns on the perceived complexity of a shape are reported by Thomas [7]. In [8], Arnoult uses the form factor, along with number of independent sides, angular variability and symmetry, to account for the judgments of the complexity experiments on humans. A recent experimental work on predicting perceived visual complexity of abstract patterns using computational measures is reported in [9] where mirror symmetry is found to be an important predictor of complexity. Since these works report results from experiments on humans[1], they represent the *perceptual* shape complexity.

It is seen that both geometrical and perceptual accounts of shape complexity consider circles to be the simplest shapes. This raises the question “why circles?".

1.1.1 Circles: the simplest shapes, traditionally

Primary motivation for considering circles, or spheres, as the simplest shapes is that physical forces tend to form these shapes. For example, the moon and the sun are spherical, as other celestial objects that can be observed with the naked eye. Larger snowballs form by rolling a smaller one on a snowy surface, further, under certain conditions, snowballs can form on their own. Occasional bumps on an angled object is more likely to occur at its bulges, forcing it to be more spherical.

Observations of such phenomena by humans have formed the biases of human vision towards comprehension of matter, deeply. So deeply that, much before axiomatizing the properties of circle, humans were able to utilize them by inventing the wheel.

[1] For a detailed review of visual complexity with emphasis on psychological studies, the reader is referred to [10].

The geometric definition and properties of circle bring forth another motivation for it to be considered as the simplest shape: it is maximally symmetric, has uniform curvature and can be identified by just a center and a radius. The maximal symmetry of circle especially reinforces the idea of the simplest shape in terms of the human vision.

Later, with the foundation of information theory, the property of being identified by just a center and a radius, from which the center can be disregarded as it does not have an effect on circleness, made explicit that a circle can be represented with minimal amount of information, the radius alone.

1.1.2 Problems

Methods based on the assumption of circles being the simplest objects, however, yield inconsistent results when implemented.

In [11], Rosenfeld shows that the form factor is not minimized by digital circles, but rather for octagons or diamonds, depending on how the perimeter of shape is measured.

Another measure that attains its minimum for circles is Danielsson's shape factor which theoretically has a minimum value of one [12]. However, in [13] a digital cross is shown to attain a value lesser than one.

A similar result for a measure that theoretically attains its minimum for circles is given in Sec. 4.3. There, it is shown that a square attains a lower complexity score than a circle when computed.

Then, the indicated problems with such methods are twofold: first, they are not minimized by digital circles, second their behavior can change with how concepts like perimeter are computed. As a result, the measurements are inconsistent.

1.2 Discrete Space versus Continuous Space

Even though circle's simplicity is well-founded, methods based on this foundation fail to evaluate the digital circles as the simplest objects and yield inconsistent results. The problem has to do with the different structures of the spaces in which the methods are *developed* and *implemented*. One is continuous and the other discrete. On one, calculus can be invented, on the other approximated. Furthermore, digital computers are limited physically and have finite resources. Therefore, methods based on the consideration of circles as the simplest shape remain as ideals whose implementations in the non-fitting media fall short of consistency and preciseness.

Notions of continuous space, such as perimeter, do not extend trivially to the discrete space [14]. Nor does the idea of circles. In the discrete space, any realization of circle violates the defining properties of circle. For example, having equidistant (as measured by the Euclidean metric) boundary points to an enclosed point is left unsatisfied due to the lack of corresponding points in space. Similarly, it is not possible to satisfy the property of having uniform curvature, for curvature does not extend properly to the discrete space either.

1.2.1 Squares: the simplest shapes in the discrete space

In the discrete space, there are shapes that can be approximately represented without losing their properties. These are the rectangles whose sides are parallel to the grid axes. However, although an approximation to such a rectangle is again a rectangle, in general, it is not *the same* rectangle. For example, the aspect ratio of the approximated rectangle can be distorted.

Of specific interest among rectangles are the squares, for the properties of being a square, which involves the aspect ratio, is left unchanged upon approximations. This is regardless of how the notion of length is defined in the discrete setting. Since the ideal square and the constructed square carry the same properties, and given the grid axes, a square can be described by just a side length, we consider the squares as the natural simplest shapes in the discrete space. Remark also that squares satisfy the property of being equidistant (as measured in L^∞) to an enclosed center.

1.3 Relative Nature of Shape Complexity

Complexity is relative, and so is the shape complexity. In this thesis, the relative nature of shape complexity is addressed in two aspects. The first is that dictated by the structure of the space. Continuous versus discrete space discussions and consideration of squares as the simplest shapes fall under this aspect. The second is that due to bias. This bias might be caused by exposure to objects of similar shapes, or by practical concerns such as having a machine capable of producing certain shapes with more ease than others.

In contrast to the objective first aspect, the second aspect is subjective. Should the subjective biases not agree with each other on the order between the shapes based on the perceived complexities, the linear order fails to be established on the shapes. For example, if the complexity is perceived in terms of boundary regularity and symmetry, it is possible that a shape with more regular boundary to have less symmetry compared to another shape.

1.4 More on Computational Literature

Vast majority of the related literature is on roundness.

Due to several shortcomings of the form factor, many other measures, similar in the spirit to the form factor, are proposed. A review of them is given by Montero and Bribiesca [13].

Several roundness measures (circularity, ellipticity) are proposed by Rosin [15]. Maragos [16] used multiscale morphological openings and closings with convex structuring elements to obtain entropy-like shape-size complexity measure. Page *et.al.* [17] associated shape complexity with entropy of boundary curvature. Chen and Sundaram [18] use correlates of Kolmogorov complexity on shape features such as boundary curvature, and promote designing efficient shape rejection algorithms that incorporate shape complexity. Ritter and Cooper [4] propose a measure of circularity that induces orders which are preserved under changes in resolution on shapes. Genctav and Tari propose a multi-scale measure of circularity [19] and a local measure of deviation from a disc [20].

Methods measuring rectangularity and squareness are proposed by Rosin [21, 15], and by Rosin and Žunić [22, 23].
Historically, relativistic rectangle discriminability is addressed in [24].

Quantifying rectangularity is emerging as a specific interest due to applications. These include, but are not restricted to, urban planning and landscape ecology [25], road extraction [26], proper alignment of parts on a robotic production line and image segmentation.

1.5 Outline

The first aspect of relative nature of shape complexity -the structure of the space in which shapes are represented- is addressed in Chapter 2. We argue that this structure defines a *natural* simple shape, and study the case for digital domain in Chapter 2. This is achieved by constructing a field -which could be considered as a well-behaving chessboard (L^∞) distance transform- inside shapes. The field is given by a differential equation whose differential part is governed by the infinity Laplacian (the Laplacian in L^∞). The Shannon entropy of the distribution acquired by restricting the constructed field to the level sets of the chessboard distance transform is then considered as the complexity of the shape.
In Chapter 6, by giving an analytical solution to this differential equation, the connection between the proposed field and the chessboard distance transform is shown. The interested reader may jump to Chapter 6 right after reading Sec. 2.2.

The second aspect of relativity -that arising from bias- is studied under Chapter 3 by reducing this kind of relativity to the question of "given a shape that is considered simple, what are the complexities of other shapes?". This is achieved by extending the method of Chapter 2 by replacing entropy with a relative entropy measure.

In Chapter 4 comparisons between entropy and relative entropy measurements in L^∞ and in Euclidean space are presented.

Since complexity is not well-defined, it is not possible to devise measures that attribute absolute scores of complexity to shapes. Because of this, complexity of shapes

cannot be mapped to real numbers, that is, a linear order on shapes cannot be induced by their complexity scores. Instead of a linear order, by using multiple measurements of complexity, it is possible to construct a partial order on shapes. This is examined under Chapter 5.

CHAPTER 2

ENTROPY MEASUREMENTS IN L^∞

2.1 Motivation

Although the consideration of circles, as simplest shapes is legitimate in ideal settings and has profound connections with physical reality, it is not in accordance with the computational view. Primary reasons for this dissonance are the finiteness of computer memory and prevention of the realization of circles, a task that demands infinite precision, by the abstraction of computer memory as a subset of $\mathbb{Z}^n$.

Even though circles can be realized approximately in the digital setting, its defining properties, such as uniform curvature and having equidistant boundary points to an enclosed point, are left unsatisfied. As a result, methods that measure complexity of shapes in reference to circles do not yield the expected result for circles when implemented in computer. It is also possible for such methods to assign lower complexity values to shapes other than circles than that assigned to circles. Consequently, they are inconsistent.

On the other hand, approximations to rectangles whose sides are parallel to the chosen axes yield rectangles. As such, measuring complexity in reference to a rectangle is expected to be less prone to the cause of inconsistency seen in methods aiming to quantify circularity.

2.2 Method

Starting with the following observations in Euclidean setting:

– For a shape S, its distance transform's successive upper level sets correspond to its successive erosions using disc structuring element.

– If we shrink shape boundary ∂S by moving its points where the distance traveled in the direction of inward normal is proportional to the boundary curvature at the point, the boundary deforms towards a curve of uniform curvature, *i.e.*, a circle. The regions closed by successive shape boundaries are *adaptive* erosions and form a multi-scale shape representation.

– For a shape with uniform boundary curvature namely disc, the distance transform's upper level sets agree with adaptive erosions. As the shape deviates from disc, the discrepancy between the respective sets increase. The discrepancy is higher for those sets that are nearer to boundary and lower for those sets that are nearer to center.

Suppose we are able to embed boundaries of successive adaptive erosions as level sets of a field f on S. Then the congruency between f and the distance transform can be measured by how uniform f is at a level set of distance transform. If S is a disc, then the restriction of f to a level set of the distance transform will be uniform. In this setting, the normalized (rescaled to $[0, 1]$) distance transform t serve as a natural scale parameter because in the direction of increasing t the level sets of f take more circular form due to adaptive erosions. It can be said that the field implicitly encodes curvature, and in fact in Euclidean setting, it correlates with curvature. However, the concept encoded by such a field is more primitive than curvature. The field construction can be extended to spaces other than Euclidean. In that case, the field encode some other concept, e.g. of having $90°$ angles.

The proposed method has two components:

1. construction of field f in the proper space whose unit balls have the desired reference shape;

2. measurement of the uniformity of the restriction of f to a certain level of t acquired in the proper metric space, *i.e.* entropy of the distribution.

The ideal simple shapes that can be realized in $\mathbb{Z}^n$, which we consider as a more

suitable space for computation as discussed in Sec. 2.1, are rectangles. Therefore, a proper space should be chosen such that the level sets of f and t for a rectangle should agree with each other. We employ L^∞ as one such proper space, since its unit balls are squares.

To avoid later confusion, the constructed field f is referred to as f_S^∞, where the superscript indicates that the field is constructed in L^∞ and the subscript indicates that it is constructed for shape S. Similarly, distance transform is referred to as t^∞.

2.2.1 Constructing f_S^∞

The field constructed by the proposed linear diffusion equation in [27]

$$\left(\Delta - \frac{1}{\rho^2}\right) f = -1 \text{ subject to } f\Big|_{\partial S} = 0 \tag{2.1}$$

is a field that embeds the boundaries of successive adaptive erosions as its level sets, as demanded. Yet, the embedded erosions are those acquired by a disc structuring element. This is due to the chosen metric, the Euclidean metric, whose minimizer is a disc. However, since the only term responsible for encoding metric information in Eq. (2.1) is the Laplace operator, it is replaced by the infinity Laplacian [28]. The PDE to be solved in S then becomes

$$\left(\Delta_\infty - \frac{1}{\rho^2}\right) f_S^\infty = -1 \text{ subject to } f_S^\infty\Big|_{\partial S} = 0 \tag{2.2}$$

where Δ_∞ is the Laplace operator in L^∞. We note that $\Delta_\infty g$ is the minimizer of $\int |\nabla g|^p$ as $p \to \infty$. Parameter ρ is chosen proportional to the shape radius as measured in L^∞. This choice ensures the robustness of solutions under changes in scale. After its construction, f_S^∞ is normalized to $[0, 1]$, which renders the constant on the right hand side of Eq. (2.2) devoid of meaning, so long as the sign is preserved. To acquire numerical solutions, the first order approximation to Laplace operator in L^∞, as given by Obermann [29] under the assumption of equidistant grid points

$$\Delta_\infty f_S^\infty(x) \approx \left(\max_{y \in B(x)} f_S^\infty(y) + \min_{y \in B(x)} f_S^\infty(y)\right) - 2 f_S^\infty(x) \tag{2.3}$$

is used, where $B(x)$ denotes a unit ball centered at x. Note that the expression Eq. (2.3) corresponds to difference between forward and backward morphological derivatives [30, 31].

Points at a system governed by Eq. (2.2) *generates* and *cumulates* the values of field. Each point introduces an increment to the neighborhood *average* (which is proportional to $(\max f_S + \min f_S)$ in L^∞ [32]). Amount of increment is decided by the screening parameter $1/\rho^2$. This increment creates level sets increasing away from the boundary and these level sets can be viewed as embeddings of gradual deformations of ∂S towards a curve possessing features of the reference shape as determined by the ball of chosen metric space. The maximum value of field is attained at the points with maximum distance to the boundaries, as they are the points of most cumulation.

An illustration of the level sets of the constructed fields is given in Fig. 2.1 that are acquired in (a) L^∞ and (b) L^2. The level curves in (a) becomes locally flat whereas the ones in (b) gets rounder. For solutions in L^2, this behavior was shown in [27] to be related to the curvature of level sets, such that at points of higher curvature propagation along the normal direction is faster than points of lower curvature.

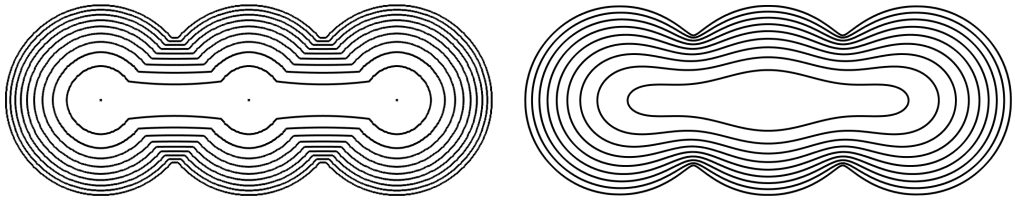

(a) (b)

Figure 2.1: Local behavior of L^∞ versus global behavior of L^2

In Fig. 2.2, the effect of the simplest (rectangular) appendages on a square-shaped body is displayed. These appendages affect the field only in a region determined by their widths. Outside these regions, appendages are disregarded.

2.2.2 Measuring multi-scale congruence

After constructing f_S^∞, normalized distance transform t^∞ inside S is acquired. This is followed by partitioning values of f_S^∞ at a level set of t^∞ into a fixed number of bins (in our implementation, 1024). A pseudo probability distribution is acquired by normalizing the count in each bin. Then the Shannon entropy at level set $t^\infty = t_0$, E_{t_0}, of this distribution is calculated as the complexity of shape S. The process

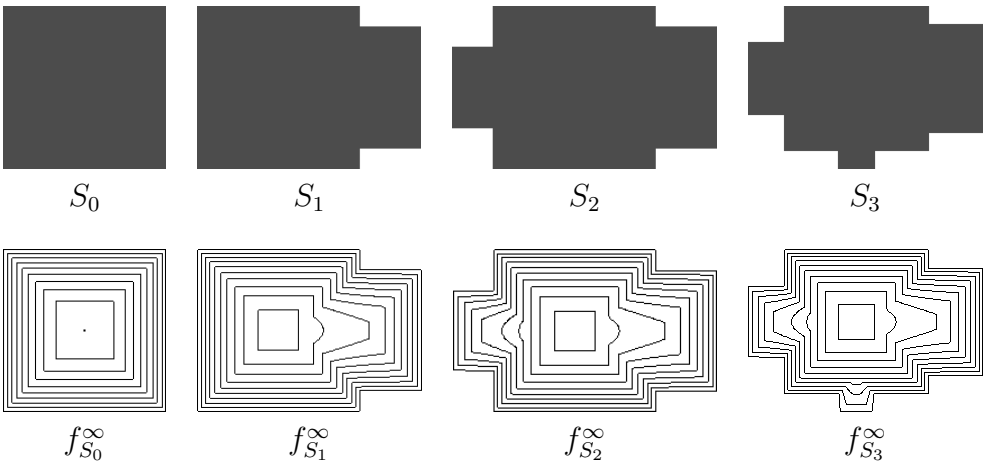

Figure 2.2: Successive addition of rectangular appendages to S_0 (square of edge width 128 pixels) and the acquired field solutions in L^∞. Introduced appendage is of width 96 pixels for S_1, 64 pixels for S_2, and 32 pixels for S_3.

is visualized in Fig. 2.3 using S_3 of Fig. 2.2; the black lines correspond to level sets of f^∞_S at $0.01, 0.3, 0.6, 0.9$, and blue dotted lines correspond to those of t^∞ at $0.2, 0.5, 0.8$.

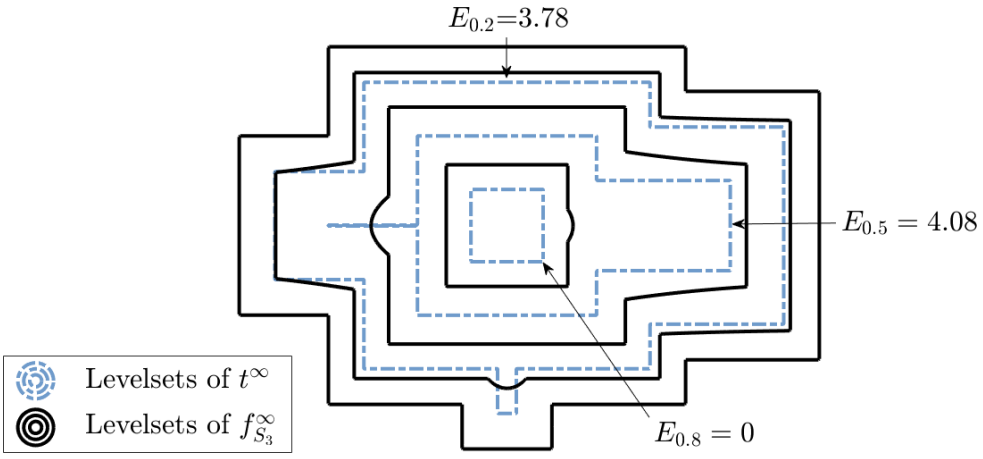

Figure 2.3: Measuring complexity in L^∞

Note that the field f^∞_S can be regarded as a *well-behaving chessboard distance transform* as will be shown rigorously in Chapter 6. Its level sets agree with level sets of distance transform whenever the boundary ∂S is isotropic in the sense of chosen metric. The discrepancy between f^∞_S and t^∞ is due to the smoothed propagation of level sets of f^∞_S in comparison to those of t^∞.

An important property observed in f_S^∞ that is not present in f_S^2 (the field governed by Eq. (2.1) and constructed in L^2) is the presence of a level for appendages beyond which the effect of the appendage of the field disappears. This level is called *a cutoff level t_c of an appendage*. t_c is not an intrinsic number of a shape, rather it emerges from appending a shape to another. t_c is determined by the ratio of *contacting width* of the appendage to the width of the main body.

The discrepancy between f_S^∞ and t^∞ is observed to reach its local maximum around t_cs. To see this, consider the level set $t^\infty = 0.5$ of Fig. 2.3. Outgrowth on the left side of this level set crosses numerous level sets of $f_{S_3}^\infty$, whereas, for $t^\infty > 0.5$ corresponding level sets of t^∞ and $f_{S_3}^\infty$ are in agreement locally on this side. Therefore, $E_{0.5}$ is significantly higher than $E_{0.5+\epsilon}$. Similarly, for $t^\infty < 0.5$, deviation of t^∞ from $f_{S_3}^\infty$ is lower. As a consequence, complexity reaches a local maximum at $t^\infty = 0.5$.

2.3 Implementation Details

Discretizing Eq. (2.2), we obtain

$$\max_{y\in B(x)} f_S^\infty(y) + \min_{y\in B(x)} f_S^\infty(y) - \left(2 + \frac{1}{\rho^2}\right) f_S^\infty(x) + 1 = 0 \tag{2.4}$$

The field f_S^∞ is constructed using the explicit scheme

$$\frac{f_S^{(k+1)}(x) - f_S^{(k)}(x)}{\Delta k} = \max_{y\in B(x)} f_S^{(k)}(y) + \min_{y\in B(x)} f_S^{(k)}(y) - \left(2 + \frac{1}{\rho^2}\right) f_S^{(k)}(x) + 1 \tag{2.5}$$

where $f_S^{(k)}(x)$ is the constructed field at the kth step, and $f_S^{(0)} \equiv 0$. Convergence conditions imposed on this scheme are

1. maximum absolute value, $\max|\Delta f_S^{(k)}|$, of RHS of Eq. (2.5) is below some threshold, ϵ_1,
2. $\max|\Delta f_S^{(k+1)} - \Delta f_S^{(k)}| \leq \epsilon_2$

In our implementation $\epsilon_1 = N \times 10^{-7}$ and $\epsilon_2 = N \times 10^{-11}$ are used where N is the number of nonzeros of the shape.

We can improve this solution by using our insight about the correlation of f_S with the distance transform, and construct a systems based solution. In doing so we use the distance transform of S in L^∞ to guide us about the locations of local maxima and minima of each point. With this initial guess, we construct $A\vec{x} = b$ where A is a sparse matrix and solve for $\vec{x}$. Pointwise error of the acquired solution is calculated using the LHS of Eq. (2.4), and this error is fedback to $\vec{x}$. This process is iterated by using the $\vec{x}$ acquired in the last step as our next guess about the location of local maxima and minima. Convergence condition for the iteration on the systems solution is either having

1. $\max \Delta f_S^{(k)} = 0$, or
2. $\max |\Delta f_S^{(k+1)} - \Delta f_S^{(k)}| \leq \epsilon_3$

In our implementation $\epsilon_3 = N \times 10^{-7}$.
Since correction of small errors via systems solutions is more costly than correction via the purely iterative scheme, ϵ_3 is chosen to be greater than ϵ_2. If the iteration on systems solution converged with the second convergence condition, acquired solution is passed to the purely iterative scheme as the initial condition.

2.4 Sample Results

In presented figures that display complexity order of shapes, single arrows are from simpler shapes to more complex shapes, and double arrows indicate equal complexity scores. Whenever there is equivalence among a group of shapes, the equivalent shapes are displayed inside a rectangular box.

The first experiment is designed to demonstrate the use of multi-scale measurements in L^∞. Three shapes are constructed by successively adding appendages of widths 96, 64, and 32 pixels to a base square with side length 128 pixels. The first order, displayed in Fig. 2.4 (a), holds for all $t^\infty \in \{0.01, 0.02, \ldots, 0.25\}$, where $t = 1/4$ is the cutoff level for appendages of interacting surface width 32 pixels when appended to a shape of radius 128 pixels. The second order, Fig. 2.4 (b), holds for all $t^\infty \in \{0.26, 0.27, \ldots, 0.50\}$. At this level $f_{S_2}^\infty$ and $f_{S_3}^\infty$ are the same and are more

complex than the other two shapes. Fig. 2.4 (c) and (d) display the orderings for $t^\infty \in \{0.51, 0.52, \ldots, 0.75\}$ and $t^\infty \in \{0\} \cup \{0.76, 0.77, \ldots, 1.00]$, respectively. Plots of entropy measurements versus t^∞ are given in Fig. 2.5.

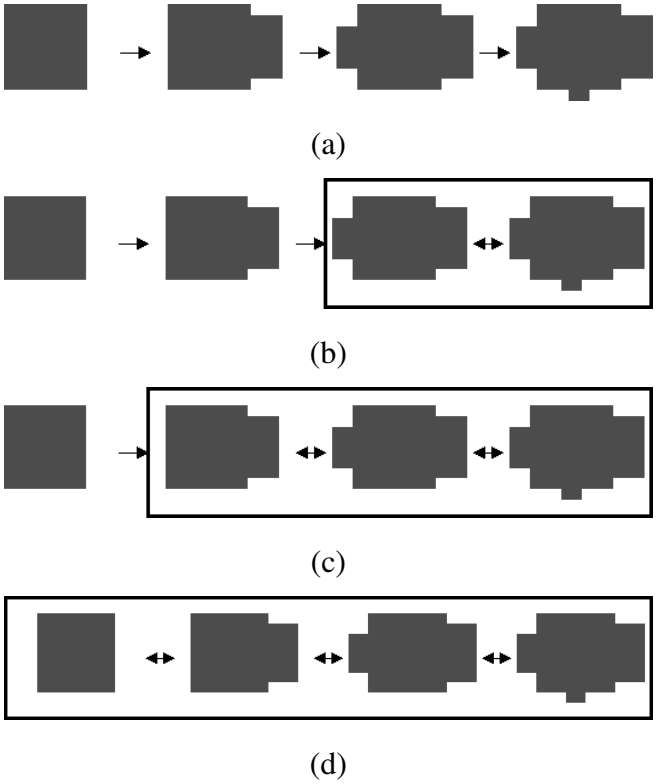

Figure 2.4: Multi-scale orderings of squares with rectangular appendages

In the second experiment, we consider a set of four rectangular shapes obtained by adding four appendages to a base square at a variety of positions. We experiment by uniformly varying t^∞. The ordering based on values collected near boundary, *i.e.* for small values of t^∞, is shown in Fig. 2.6 (a). The first shape has the lowest whereas the other three share the same complexity score. The behavior is uniformly observed for $t \in \{0.01, 0.02, \ldots, 0.25\}$. As t^∞ increases further, all four shapes attain the same complexity score (Fig. 2.6 (b)). Recall that effects of protrusions are local in L^∞ solutions. Hence, any irregularity caused on the field occurs around joints. Since the shapes introducing sixteen corners (the last three shapes) are indistinguishable from one another locally around joints, they have the same complexity scores. The shape that introduces twelve vertices (the first shape from left), however, can be told apart based on its local properties: it has only four joints, in contrast to eight joints of the other three shapes.

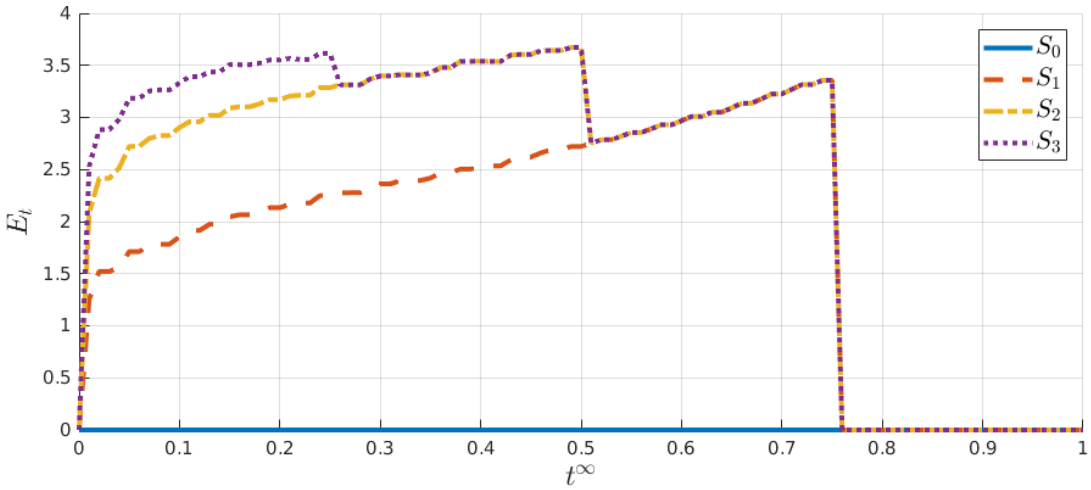

Figure 2.5: Complexity scores of S_0, S_1, S_2 and S_3 of Fig. 2.2 versus the scale parameter

This result can be interpreted in terms of the physical process of joining smaller squares to a larger square. In doing so, one can either use an existing corner, or find a specified point along the edge to use as the joint point of the squares. Locating a new point would require more effort than using an existing point, therefore, is a more complex process.

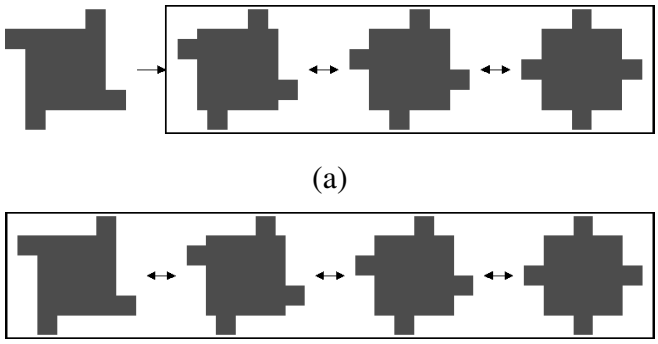

(a)

(b)

Figure 2.6: Multi-scale orderings of squares of varying locations of rectangular appendages

In the third experiment, we observe the joint effect of the placement, size and number of appendages. We construct a set of shapes by varying these three properties. The appendage placement is chosen in two ways: at the center or the corner. The size (width) of appendages is also chosen in two ways: 32 or 80 pixels. Finally, the number of the appendages is chosen in three ways: $1, 2$ or 4. Ordering obtained by our method using values collected at $t^\infty \in \{0.01, 0.02, \ldots, 0.25\}$ is shown in Fig. 2.7 (a).

The order is based on the number of appendages first, and between equals, width of appendages is taken into account. That is, it induces a dictionary order. Ordering obtained using values collected at $\{0.26, 0.27, \ldots, 0.62\}$ is shown in Fig. 2.7 (b). At this scale all shapes with 32 pixel width appendages attain the same complexity score, 0. Finally, ordering induced using values collected at $\{0\} \cup \{0.63, 0.64, \ldots, 1.00\}$ is shown in Fig. 2.7 (c). Here, all shapes attain the same complexity score.

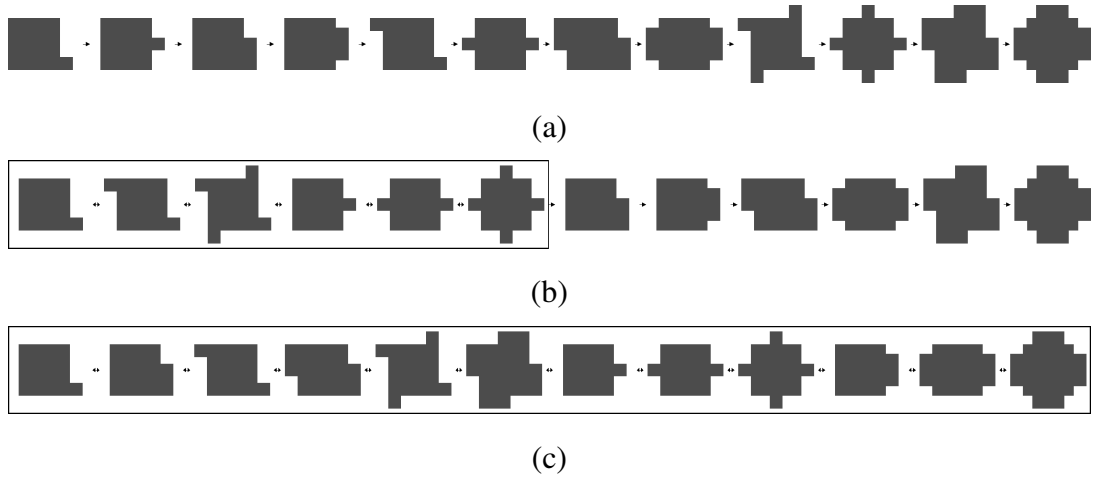

(a) (b) (c)

Figure 2.7: Multi-scale orderings of squares with varying number, width and location of rectangular appendages

Next, a real-life rectangular shape example, a house plan (P_4), is considered. As simpler references, shapes P_0, P_1, P_2 and P_3 are constructed. Boundaries of these shapes are displayed in Fig. 2.8. P_0 is a plan of four disconnected identical rooms of side lengths 128 pixels, P_1 is constructed by connecting the rooms with apertures of 32 pixels, P_2 is constructed by adding an obstacle to one of the rooms aligned with the vertical aperture and of size 32×4 pixels, and P_3 is constructed by expanding the length of apertures of P_2 to 80 pixels. As more complex references two bat silhouettes taken from MPEG7-dataset are used.

In Fig. 2.9 complexity scores of these shapes are shown. The complexity of P_4 is higher than that of P_0, P_1, and P_2 at all scales, and is lower than that of bat_{10} and bat_{20} at all scales except at $t^\infty = 0.95$ where the complexity of P_4 is higher than bat_{10}'s. The complexity of P_3 is higher than P_4's at $t^\infty \in \{0.44, 0.45, \ldots, 0.62\}$ and drops to 0 at $t^\infty = 0.63$. This drop is explained by the cutoff level $t_c = 0.625 (= 80\text{px}/128\text{px})$

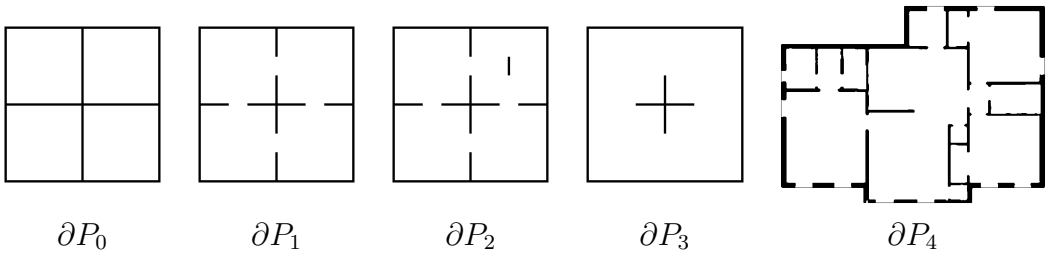

Figure 2.8: House plan P_4 and simpler shapes of similar properties.

of the apertures of P_3.

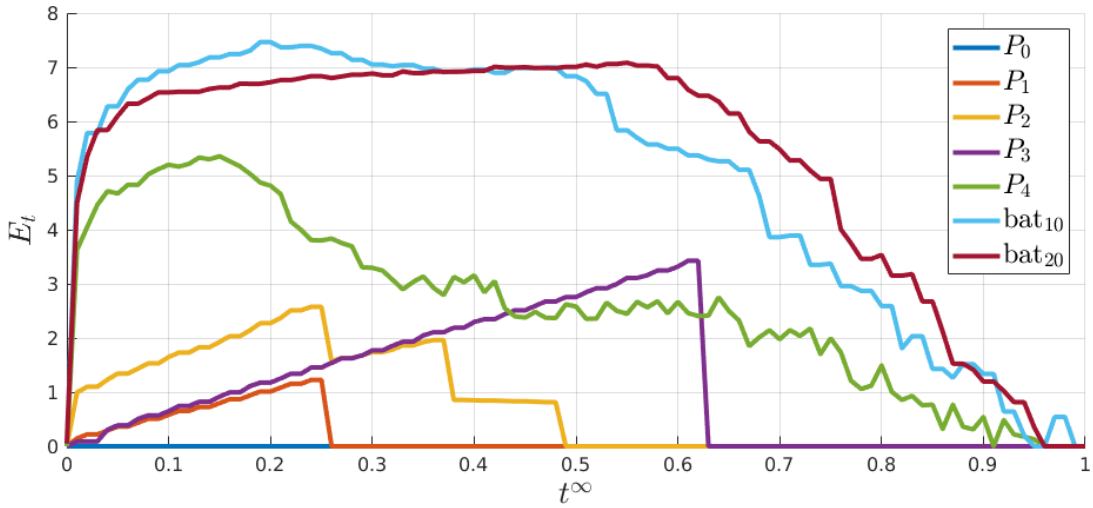

Figure 2.9: Complexity scores of a house plan, its four simpler versions and two bats taken from MPEG7 dataset versus the scale parameter

2.4.1 Noisy shapes

Fifty random datasets are created by adding noise to a square of side length 128 using a stochastic noise addition algorithm with differing amount of noise ($\# \in \{50, 100, 150, 200\}$), and varying noise factors ($nf \in \{1/64, 1/32, 1/20, 1/16\}$), which results in sixteen shapes in each of the datasets. The noise factor nf determines the width and height of noise stochastically based on the radius of shape. Pseudocode is given in Algorithm 1. The function `normRand` returns random numbers from the normal distribution. It takes mean μ of the distribution as its first parameter, standard deviation σ as its second parameter, and a third parameter that determines how many

numbers are output. The functions `drawLinesX` and `drawLinesY` add noise in outwards x and y directions from a random point on shape boundary.

Two of the created datasets are shown in Fig. 2.10.

Algorithm 1 Noise generation

function ADDNOISE(S, nf)

$\mu \leftarrow nf \times$ GETSHAPERADIUS(S)

$width \leftarrow$ NORMRAND(μ, $\mu/3$, 1)

$x_n \leftarrow$ NORMRAND(μ, $\mu/3$, $width$)

$y_n \leftarrow$ NORMRAND(μ, $\mu/3$, $width$)

$P \leftarrow$ POINTONBOUNDARY(S)

$S' \leftarrow$ DRAWLINESX(S, P, x_n)

$S' \leftarrow$ DRAWLINESY(S', P, y_n)

$S' \leftarrow$ MORPHOLOGICALCLOSING($S', square_\mu$)

return S'

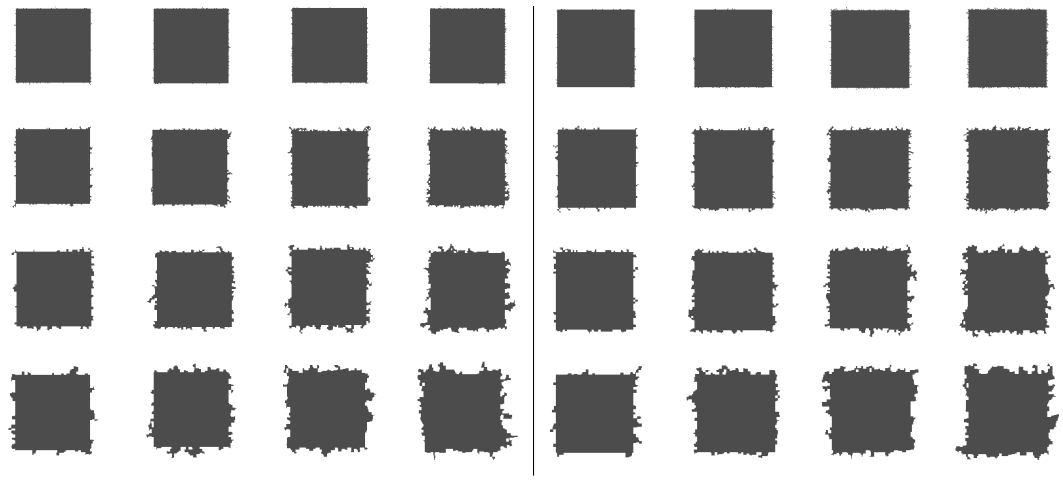

Figure 2.10: Two of fifty datasets consisting of sixteen noisy squares

In the first experiment, we fix the noise factor and then at each noise factor calculate modified Kendall τ correlation between the expected order (*i.e.* the order with respect to number of noise applications) and the obtained order. Correlations are calculated for all fifty random datasets. The top four rows of Table 2.1 show the results for each noise factor. The entries are the averaged modified Kendall τ scores. Respective standard errors of the estimation are depicted in the top four rows of Table 2.2.

We note that the modified Kendall τ returns $+1$ for equal pairs regardless of the reference ordering. This is motivated by the equal complexity scores arising only for the complexity score of 0, meaning that the noise is completely disregarded.

Table 2.1: Averages of modified τ correlation coefficients of entropy measurements in L^∞ over the fifty datasets of noisy squares

nf \ t^∞	0.1	0.2	0.3	0.4	0.5	0.6	0.7	0.8	0.9
1/64	1.00	1.00	1.00	1.00	1.00	1.00	1.00	1.00	1.00
1/32	0.82	0.95	1.00	1.00	1.00	1.00	1.00	1.00	1.00
1/20	0.96	0.94	0.92	0.94	1.00	1.00	1.00	1.00	1.00
1/16	1.00	0.95	0.87	0.85	0.88	0.93	0.98	1.00	1.00
# \ t^∞	0.1	0.2	0.3	0.4	0.5	0.6	0.7	0.8	0.9
50	0.99	0.99	1.00	1.00	1.00	1.00	1.00	1.00	1.00
100	1.00	1.00	0.99	0.99	1.00	1.00	1.00	1.00	1.00
150	1.00	0.98	0.98	0.98	1.00	1.00	1.00	1.00	1.00
200	1.00	0.99	0.98	0.99	1.00	1.00	1.00	1.00	1.00

Table 2.2: Standard deviations of modified τ correlations of entropy measurements in L^∞ over the fifty datasets of noisy squares

nf \ t^∞	0.1	0.2	0.3	0.4	0.5	0.6	0.7	0.8	0.9
1/64	0.00	0.00	0.00	0.00	0.00	0.00	0.00	0.00	0.00
1/32	0.22	0.12	0.00	0.00	0.00	0.00	0.00	0.00	0.00
1/20	0.11	0.13	0.19	0.15	0.00	0.00	0.00	0.00	0.00
1/16	0.00	0.12	0.21	0.28	0.24	0.16	0.10	0.00	0.00
# \ t^∞	0.1	0.2	0.3	0.4	0.5	0.6	0.7	0.8	0.9
50	0.05	0.05	0.00	0.00	0.00	0.00	0.00	0.00	0.00
100	0.00	0.00	0.05	0.05	0.00	0.00	0.00	0.00	0.00
150	0.00	0.08	0.08	0.08	0.00	0.00	0.00	0.00	0.00
200	0.00	0.05	0.08	0.07	0.00	0.00	0.00	0.00	0.00

In the second part of the experiment, we fix the number of noise addition (amount of noise) and then at each number calculate modified Kendall τ correlation between the expected order (*i.e.* the order with respect to noise factor) and the obtained order. The results are given in the respective bottom four rows of Table 2.1 and Table 2.2. The agreement between the induced orderings and the expected orderings increase with t^∞, which is in accordance with the claim that effects of noise are disregarded at

higher t^∞s.

Table 2.3: Modified τ correlation coefficients averaged over fifty datasets of noisy squares between rankings by $\sum E_{t^\infty}$ and rankings by control parameters for each control parameter

nf	$1/64$	$1/32$	$1/20$	$1/16$
τ	0.99	0.99	0.98	0.95
$\#$	50	100	150	200
τ	1.00	1.00	1.00	0.99

Instead of using entropy measurements at a given scale, measurements at all scales can be used. A simple way to do this is to calculate $\sum E_{t^\infty}$, a single number representing the complexity, for each shape. The modified Kendall τ scores acquired from this measurement are presented in Table 2.3.

2.4.2 Three-dimensional shapes

The methods developed in this chapter can easily be generalized to shapes of arbitrary dimensions. For the three-dimensional case, using 26 immediate neighbors of a grid point as $B(x)$ in the discretization Eq. (2.3) is sufficient to construct the field at three-dimensions. The construction of L^∞ distance transform in three-dimensions follows trivially. In this subsection, an experiment with the generalization of the method to three-dimensions is displayed.

Ten shapes are constructed by successively appending smaller cubes of side length 16 at the center of the surfaces of a larger cube of side length 64. The constructed shapes are displayed in Fig.2.11 from two views. The names of the shapes indicate the number of appendages, and their locations, if needed. Subscript a indicates a preference towards opposite surfaces when appending a smaller cube, and b indicates adjacent surfaces are preferred.

Complexity scores of these shapes are shown in Fig.2.12 for $t^\infty \in \{0, 0.01, \ldots, 0.3\}$. For $t^\infty >= 0.26$, all shapes attain a complexity score of 0. Note that $t_c = 0.25$ for the appended smaller cubes. S_0 is the simplest shape, as expected, with a complex-

ity score of 0 uniformly across all values of t^{∞} and the complexity increases with increasing amount of appendages. The location of appendages has no effect on the measured complexities, since their fields of interactions are not intersecting. These results are in alignment with the results of two-dimensional shapes.

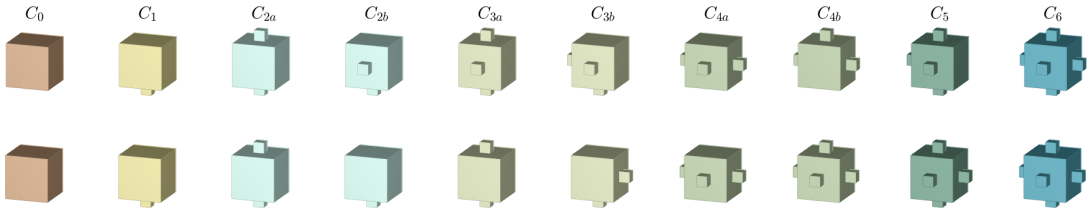

Figure 2.11: Cubes of varying number of cubic appendages. Top row: azimuthal angle of 20 degrees, elevation angle of 15 degrees; bottom row: azimuthal angle of 200 degrees, elevation angle of 15 degrees.

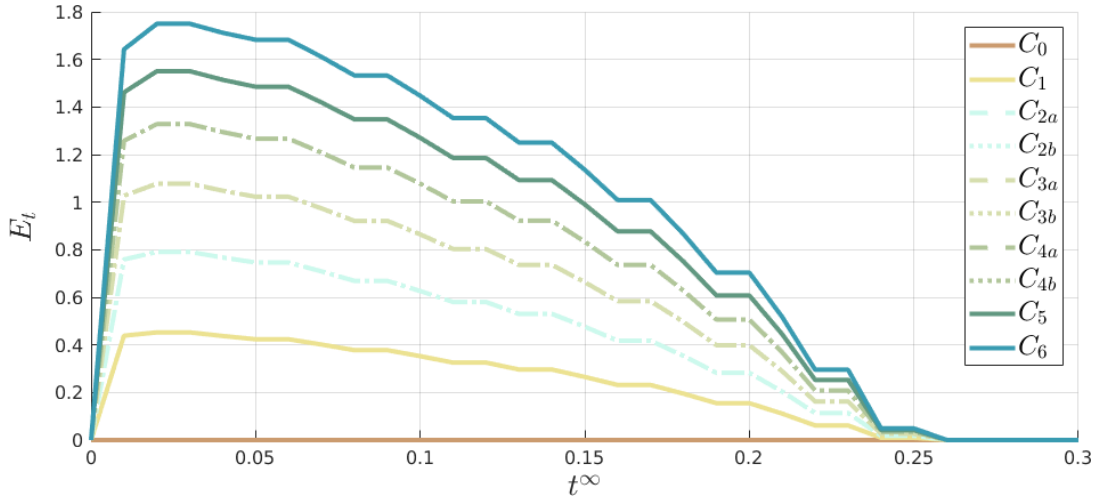

Figure 2.12: Complexity scores of cubes versus the scale parameter

CHAPTER 3

RELATIVE MEASUREMENTS IN L^∞

3.1 Motivation

Shape complexity is a relative property. Depending on which shapes are taken as simple, order of other shapes based on complexity change.

Therefore, constructing a framework that is capable of evaluating shape complexity with respect to arbitrary shapes is of importance. However, it is not easy to ensure the consistency of such a flexible framework. To overcome this, we propose a framework based on the method developed in Chapter 2, for it is built on assumptions agreeing with the discrete structure of the digital shape space.

3.2 Method

Entropy is a measure of information content of a distribution relative to uniform distribution. A more general measure can be obtained by replacing the uniform distribution (which is the reference) with a more general one. Kullback-Leibler divergence, also known as relative entropy, is one available way to measure information content of a distribution P relative to another distribution Q [33]. It is defined as

$$D_{KL}(P \,||\, Q) = \sum_{x \in X} P(x) \log \frac{P(x)}{Q(x)}.$$

$D_{KL}(P \,||\, Q)$ is defined only if $Q(x) = 0$ implies $P(x) = 0$, that is, $\operatorname{supp} P \subset \operatorname{supp} Q$. This, however, is not necessarily satisfied for arbitrary distributions. Hence, we modify $D_{KL}(P \,||\, Q)$ to address these by defining

$$D^*(P\,||\,Q) = \min_{k\in\{-d,-d+1,\ldots,d\}} \sum_{x\in\operatorname{supp} Q^{(k)}} P(x)\log\frac{P(x)}{Q^{(k)}(x)} - \sum_{x\notin\operatorname{supp} Q^{(k)}} P(x)\log P(x) \tag{3.1}$$

where $Q^{(k)}$ is the k-times *pushed* distribution and d is a small number compared to the total number of bins. In our implementation, number of bins N is $2^{10} = 1024$ and d is $2^2 = 4$ which accounts for a minimization region of $(2d+1)/N \approx 0.9\%$, and the distributions are diffused according to

$$P^{(k+1)}(x) = P^{(k)}(x) + \alpha[P^{(k)}(x-1) + P^{(k)}(x+1) - 2P^{(k)}(x)]$$

64 times prior to calculating $D^*(P\,||\,Q)$, where $P^{(0)} = P$ and $\alpha = 0.1$. Both introducing a minimization over k and diffusing the distributions aims to solve the problems due to discrete calculation of the real field f_S and its further discretization to acquire distributions.

The proposed $D^*(P\,||\,Q)$ agrees with $D_{KL}(P\,||\,Q)$ whenever $\operatorname{supp} P \subset \operatorname{supp} Q$ upto the difference due to minimization over k. Otherwise, the additional term akin to Shannon entropy penalizes P based on its nonzeros lying outside the support of Q.

3.3 Results

In this section, results acquired by using $D^*(P\,||\,Q)$ are presented under three tests. The first of these tests is done on simple shapes of squares and circles, and shapes acquired from them by appending similar shapes, respectively. In the second test, a dataset consisting of twenty shapes from MPEG7 datasets are used. Finally, we test the relative entropy with respect to the noiseless disc on datasets composed of noisy discs.

3.3.1 Test 1

In this test, we experiment with relative measurement on two datasets composed of shapes of varying number of appendages. One of the datasets is prepared by appending rectangular shapes to a square, and the other by appending circular appendages to

a disc. Appendages are positioned either at the top, bottom, right or left of the main shape. Shapes are named according to the present number of appendages, *i.e.* disc with four appendages is called D_4, and a square with four appendages is called S_4. For different possible positions of appendages subscripts a and b are used, where a indicates appendages are on opposite sides.

3.3.1.1 Squares with rectangular appendages

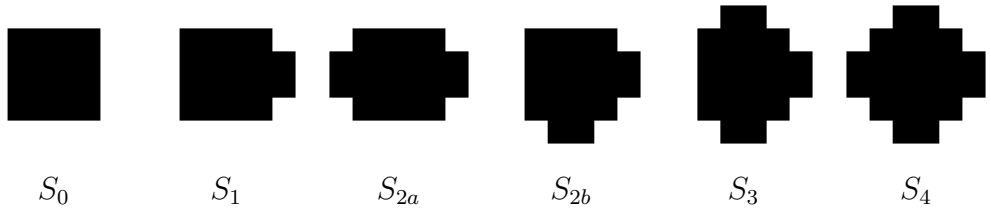

Figure 3.1: Squares with rectangular appendages

The dataset used in this part of the test is displayed in Fig. 3.1. Side length of S_0 is 256 pixels. The other shapes are acquired by successively appending squares of side length 128 pixels at the center of each side.

Measurements with respect to S_0 are displayed in Fig. 3.2. The order on shapes based on their complexities are stable for all t^∞, except $t^\infty = 0.02$, and is based solely on the number of parts at where the shapes can be distinguished from one another, *i.e.* for $t^\infty \leq 0.50$. For $t^\infty > 0.50$, all of the shapes attain the same score, since $t^\infty = 0.50$ is the cutoff level. The instability at $t^\infty = 0.02$ holds only for the order between S_3 and S_4.
The same order is also established by using entropy on this dataset as shown in Sec. 4.2.

Measurements with respect to S_4 are displayed in Fig. 3.3. This time complexity scores show stable behavior for all t^∞. Before the cutoff level $t_c = 0.5$, the induced order is based on the number of parts again, though in a reverse fashion.

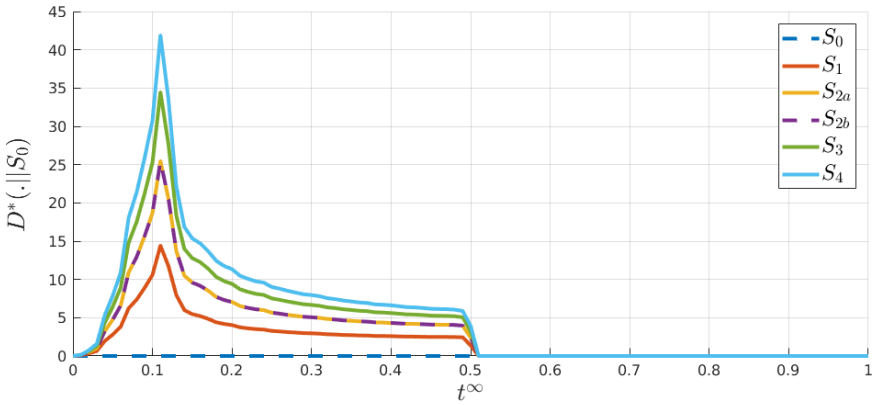

Figure 3.2: Complexities of rectangular shapes with respect to S_0

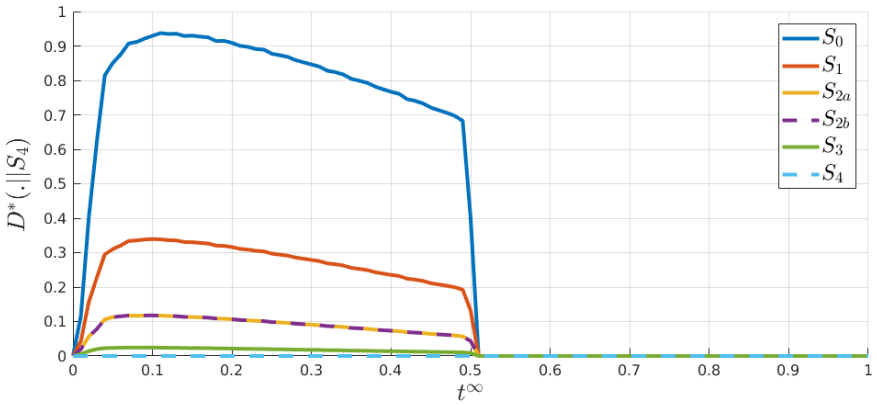

Figure 3.3: Complexities of rectangular shapes with respect to S_4

Measurements with respect to S_{2a} are not as easy to reason about as the above two measurements. For example, S_1 and S_3 could be expected to be of same complexity if it is deduced from the earlier examples that the measurements amount to counting the appendages. However, since the area between $D(S_0 \,||\, S_4)$ and $D(S_1 \,||\, S_4)$ is much higher than that between $D(S_1 \,||\, S_4)$ and $D(S_2 \,||\, S_4)$, it is clear that the behavior is not homogeneous. This, together with the observation that the area between $D(S_4 \,||\, S_0)$ and $D(S_3 \,||\, S_0)$ is lower than that between $D(S_3 \,||\, S_0)$ and $D(S_2 \,||\, S_0)$, implies that *adding an appendage is a simpler process than removing one.* The results of the measurements are displayed in Fig. 3.4. The induced order on these shapes is similar to a dictionary order that orders, first, based on the difference of the number of appendages with the reference shape, and between equals, orders based on whether an appendage is added or removed.

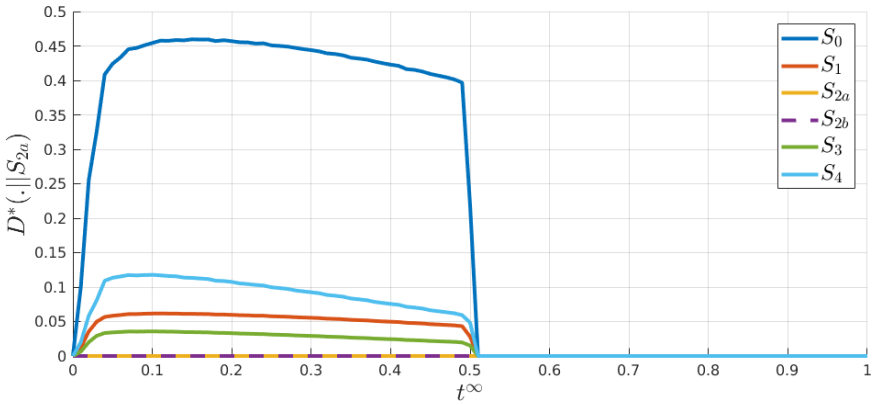

Figure 3.4: Complexities of rectangular shapes with respect to S_{2a}

Table 3.1: Integrals of complexity scores with respect to S_0, S_4 and S_{2a}

	S_0	S_1	S_{2a}	S_{2b}	S_3	S_4
$\int D^*(.\,\|\|\,S_0)$	0.00	1.95	3.36	3.36	4.48	5.38
$\int D^*(.\,\|\|\,S_4)$	0.40	0.14	0.04	0.04	0.01	0.00
$\int D^*(.\,\|\|\,S_{2a})$	0.21	0.03	0.00	0.00	0.01	0.05

Notice that the range of complexity scores changes significantly between the measurements with respect to S_0, S_4 and S_{2a}. In Table 3.1 the areas under each curve are given. Based on these scores, order of shapes with respect to S_0, S_4 and S_{2a} can be established without worrying about which interval of t^∞ should be used.

3.3.1.2 Discs with circular appendages

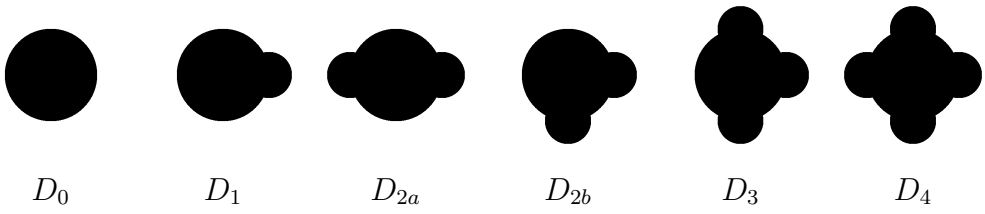

Figure 3.5: Discs with circular appendages

As the second case, discs with circular appendages are tested on. The shapes are as displayed in Fig. 3.5. They are acquired by successively appending discs of radius 64 pixels to a disc, D_0, of radius 128 pixels.

Measurements with respect to D_0 are displayed in Fig. 3.6. Plots show that the complexity of discs increases with increasing number of appendages. The order between the shapes is stable across all $t^\infty < 0.71$.

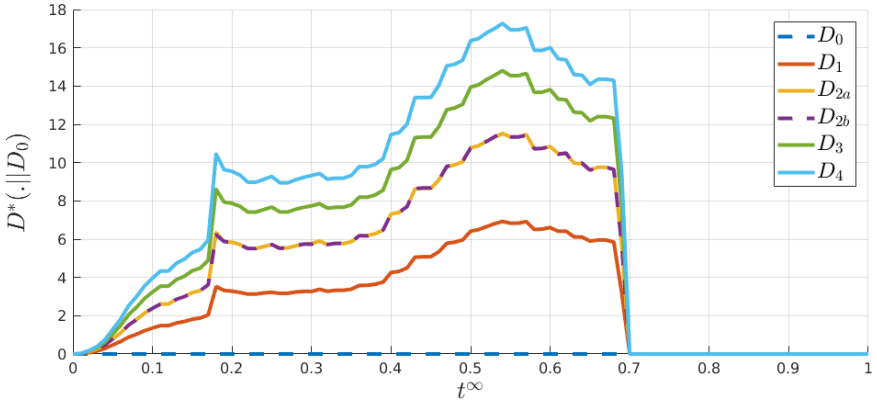

Figure 3.6: Complexities of circular shapes with respect to D_0

Measurements with respect to D_4 are displayed in Fig. 3.7. The results are similar to the results of the square equivalent: complexities of shapes decrease with increasing number of appendages.

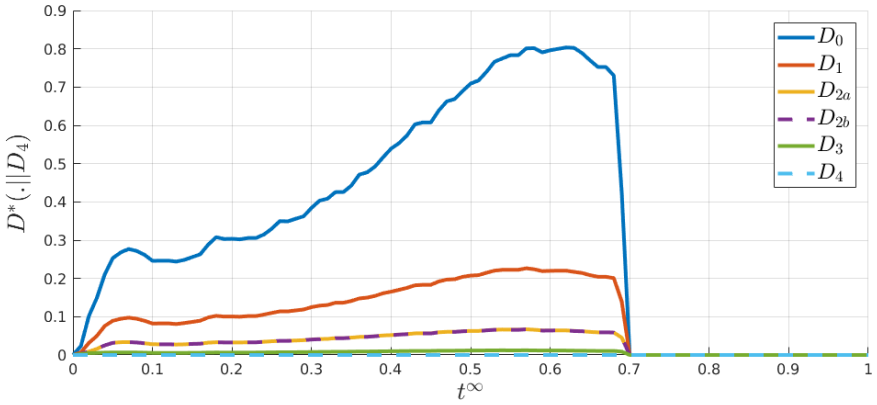

Figure 3.7: Complexities of circular shapes with respect to D_4

Measurements with respect to D_{2a} are displayed in Fig. 3.8. The expected order on the shapes is established at $t = 0.02$ and maintained until $t = 0.70$. This results are in alignment with those of S_{2a}, except here, an instability is observed at $t = 0.01$. However, keeping in mind that discs are very unnatural shapes in the imposed scheme, the results of this test can be regarded as successful.

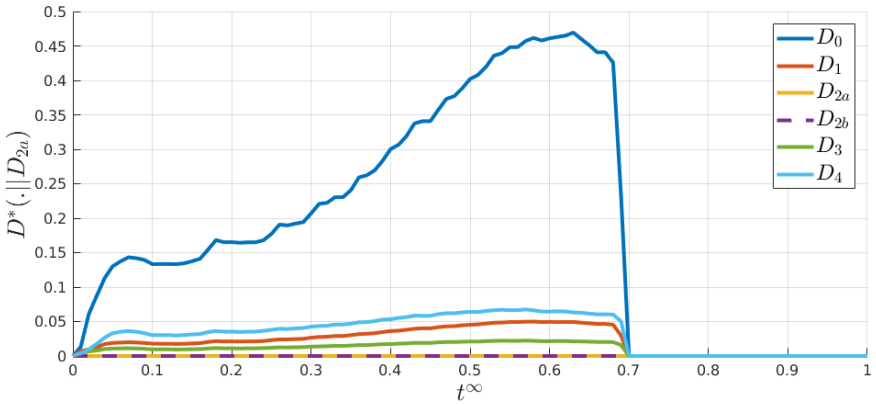

Figure 3.8: Complexities of circular shapes with respect to D_{2a}

Table 3.2: Integrals of complexity scores with respect to D_0, D_4 and D_{2a}

	D_0	D_1	D_{2a}	D_{2b}	D_3	D_4
$\int D^*(.\,\|\|\,D_0)$	0.00	2.68	4.55	4.55	5.94	7.03
$\int D^*(.\,\|\|\,D_4)$	0.33	0.10	0.03	0.03	0.01	0.00
$\int D^*(.\,\|\|\,D_{2a})$	0.19	0.02	0.00	0.00	0.01	0.03

The cutoff level for discs is observed to be $t^\infty = 0.70$. We note that this value is in accordance with the ratio of side length of maximal square that can be fitted inside a disc, and the disc's radius which is $\sqrt{2}/2 \approx 0.7071$.

Similar to the case of rectangular shapes, the range of complexity scores reduces when measurements are relative to D_4 and D_{2a}. Table 3.2 lists areas under each plot.

3.3.2 Test 2

In the second test relative measurements are made on 'device3' of MPEG7 datasets. The complexity versus scale parameter of each shape with respect to the designated reference shapes are displayed in Fig. 3.9. The median filtered results are displayed in Fig. 3.10. The first three references are chosen as the representative shapes of three groups as clustered perceptually. The other two references are chosen to compare the relative measurement with respect to shapes from the same group. To be able to discuss the result with more ease, we will refer the first three shapes as the *square*

group, fourth to eighth shapes as the *oval group*, ninth and tenth shapes as the *curvy group*, eleventh to fifteenth shapes as the *concave group*, and the rest as the *cut group*. We note that the first two shapes, S_1 and S_2, of the square group are identical. So are S_{12} and S_{13}.

Measurements with respect to the first reference shape are considered in detail for their instructive behavior.

The lowest complexity scores are acquired by the shapes in the square group. The noisy square in the group, S_3, has nonzero complexity at only small scales. There, it reaches zero at $t = 0.14$ first, and after $t = 0.37$ it is completely zero. In between these scales it attains nonzero complexity scores occasionally, although the scores at those scales are very low around 0.04.

Next, we consider the oval group. The group has varying amount of circular properties. Although the shapes in the group attain low complexity scores, none of their complexity scores reach absolute zero before $t = 0.98$. This could be because of the absence of notion of corners in these group.

It is noteworthy to mention that S_7, despite not reaching absolute zero, attains very low complexity scores (around 0.005), at mid-scales ($t = 0.45$), and maintains them at higher scales. The difference between S_7 and the others is that the presence of circularity is accompanied by protrusiveness at where the square's corners would be. In a sense, S_7 has 'fake' corners.

We also remark that for S_5 and its noisy version, S_6, the noise helps to attain lower scores at high scales, while it causes an increase at small scales. In fact, the lowest $\int D^*(. \,||\, S_1)$ in this group is attained by S_6.

The shapes in the curvy group have distinctive complexity profiles. Their complexities are similar to each other, however, S_9 is slightly more complex than S_{10} at almost all scales. We remark that this is despite the presence of corners in S_9.

For the shapes in concave group, although the complexities drop to near zero around $t = 0.3$, it is not until around $t = 0.75$ for any of them to reach the absolute zero. At small scales, it is seen that the complexity scores are much higher than those of the noisy square. The complexities increase with increasing amount of deformation.

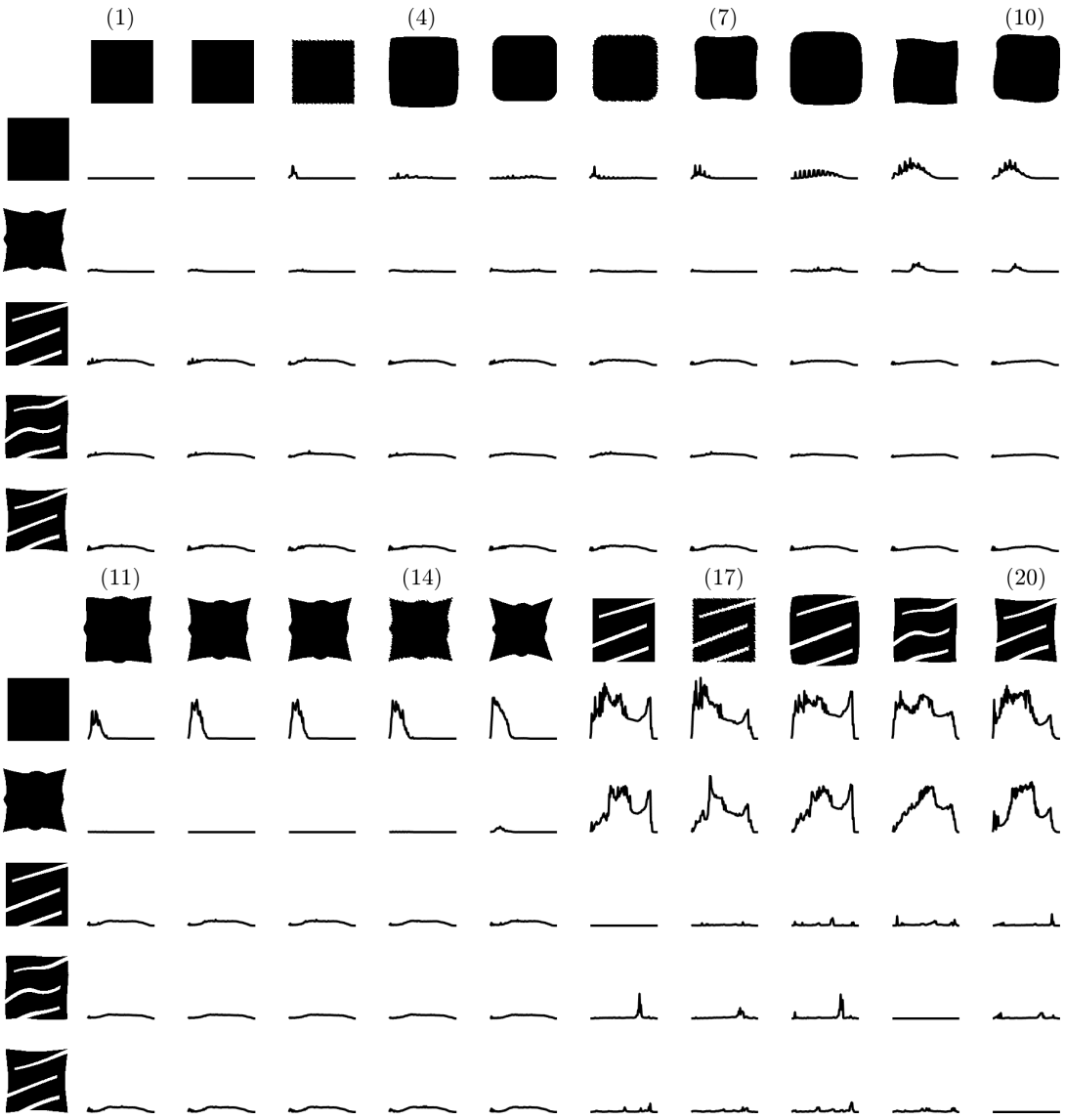

Figure 3.9: Plots of complexities for twenty shapes taken from MPEG7 dataset measured with respect to five reference shapes.

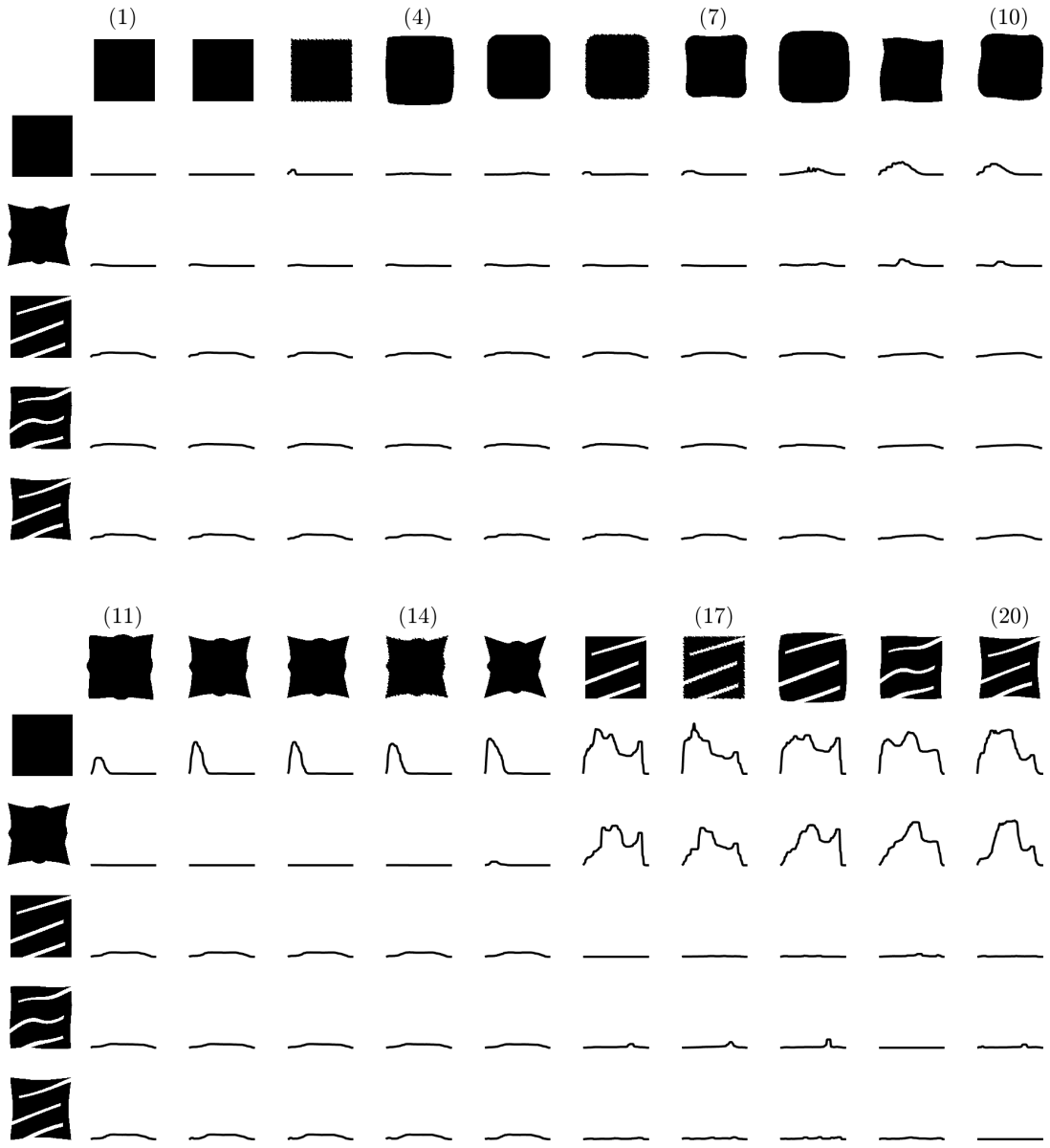

Figure 3.10: Plots of median filtered complexities for twenty shapes taken from MPEG7 dataset measured with respect to five reference shapes.

S_{11} attains the lowest complexity as measured by $\int D^*(. \,||\, S_1)$, whereas S_{15} attains the highest.
S_{13} and its noisy version, S_{14} have very similar plots. It is seen that the noise causes an increase in the shape complexity at low scales.

The shapes in the cut group have much higher complexity scores than the other shapes, and reach -or even get close to- zero at only very high scales. S_{17} has higher complexity at low scales, and lower complexity at high scales than S_{16}, similar to the case between S_6 and S_5.

Measurements with respect to the second reference shape are considered next. The first thing to mention is the general drop on the complexity scores. This is because the distributions acquired from the reference shape now has a wider support which causes most of the shapes to evade the penalty term.

Comparing S_{13} with S_{14} it is seen that the noise causes small increases at low scales, similar to the case for the complexity of S_3 as measured with respect to S_1. The most complex shape in terms of $\int D^*(. \,||\, S_{13})$ among the concave group is S_{15}, and the least -except S_{12} and S_{13}- is S_{11}. This is in line with the discussions of S_{2a} under Subsec. 3.3.1: additive deformations are regarded less complex than subtractive ones, provided they are done “in the same manner".

The curvy group, again, attains distinctive complexity profiles, for which dominant non-zero complexities are localized around $t = 0.40$. The complexity scores of S_9 is found to be greater than or equal to S_{10}'s at 61% of the probed scales. Also, the integral of complexity score for S_9 is 1.68 times that of S_{10}'s complexity score.

Among the oval group, the scores of S_5 and S_6 are noteworthy. The *noisy one is less complex* at 76% of the probed scales. In terms of the integrals of complexity scores, S_5 attains 2 times the score of S_6, which concludes that it can be considered more complex in general.
S_7 is the least complex and S_8 is the most complex of the group in terms of complexity integrals.

The complexities of the shapes in the cut group are seen to reduce at lower scales com-

pared to the complexities assigned by the first reference shape. More interestingly, at high scales, they attain the same complexity trends as they attained with respect to the first reference shape. This is because the reference shape S_{13} is basically considered as a square at high scales which is shown by $D^*(S_{13} \,||\, S_1)$.

Measurements with respect to the third, fourth and fifth reference shapes are discussed together.

Notice first that the ranges of complexity scores have reduced further. This further supports the role of spread of support of the reference shape on the range of the complexity scores, as discussed above.

The shapes that are not in the cut group attain very similar complexity profiles, in that, they attain a low complexity score at low scales, and more or less maintain it until high scales. Nonetheless, discriminative information is subtly provided. For example, the shapes in the curvy group follow a slightly positive trend until around $t = 0.70$ that is not present in the shapes of other groups. The profiles of the concave group depict low complexity scores until around $t = 0.20$, after which they attain a complexity scores which is maintained until around $t = 0.75$. For the square group, the profiles and complexity scores are almost identical to those of the concave group for $t > 0.35$. However, at lower scales the shapes in the square group attain higher complexity scores than the shapes of concave group. This indicates that near the boundary, square group is more complex than the concave group with respect to the shapes of cut group.

The profiles for the cut group change the most under changes of reference. Rather than maintaining a stable complexity score, the scores change over the scales. It is seen that S_{16}, S_{17} and S_{18} with respect to the fourth and fifth references have similar profiles. Among these shapes S_{17} attains the lowest complexity integral with respect to the fourth reference, and S_{16} attains the lowest complexity integral with respect to the fifth reference. In both cases, S_{18} is the most complex shape among these three shapes.

It is also seen that the noise of S_{17} *is not attenuated* under measurements with respect to S_{16}.

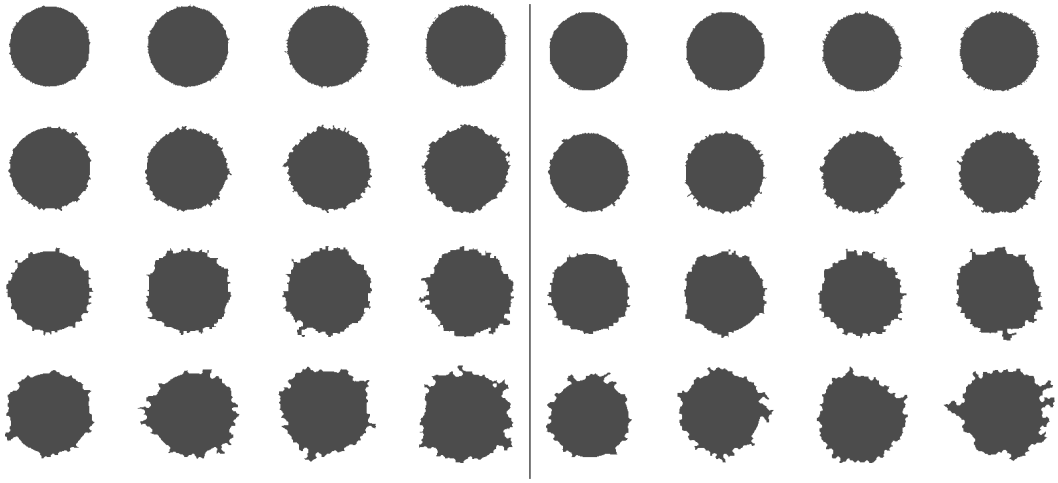

Figure 3.11: Two of fifty datasets, each consisting of sixteen noisy discs

3.3.3 Test 3

For this test, fifty noisy datasets each composed of sixteen shapes are constructed. Noisy shapes are acquired by adding noise to a disc of radius 64 pixels using the algorithm presented in Subsec. 2.4.1, except, instead of a square structuring element, a disc structuring element is used. Two of the created datasets are shown in Fig. 3.11.

Table 3.3: Averages of modified τ correlation coefficients of pointwise relative entropy measurements in L^∞ with respect to a disc over the fifty datasets of noisy discs

nf \ t^∞	0.1	0.2	0.3	0.4	0.5	0.6	0.7	0.8	0.9
$1/64$	0.86	0.87	0.77	0.72	0.67	0.68	0.55	0.63	0.49
$1/32$	0.69	0.34	0.41	0.37	0.50	0.54	0.51	0.29	0.36
$1/20$	0.73	0.62	0.08	0.20	0.09	0.13	0.10	0.27	0.17
$1/16$	0.66	0.55	0.07	0.31	0.17	0.16	0.13	0.08	0.17
$\#$ \ t^∞	0.1	0.2	0.3	0.4	0.5	0.6	0.7	0.8	0.9
50	0.94	0.85	0.71	0.75	0.71	0.77	0.76	0.76	0.61
100	0.96	0.87	0.61	0.54	0.66	0.72	0.59	0.67	0.54
150	0.96	0.83	0.47	0.61	0.51	0.70	0.63	0.59	0.47
200	0.94	0.81	0.41	0.65	0.65	0.67	0.53	0.56	0.45

Measurements relative to the base disc of radius 64 pixels are carried out. Induced order on the shapes by these measurements are expected to be based on the amount of noise.

Table 3.4: Averages of modified τ correlation coefficients of regional relative entropy measurements in L^∞ with respect to a disc over the fifty datasets of noisy discs

nf \ t^∞	I_0	I_1	I_2	I_3	I_4	I_5	I_6	I_7	I_8	I_9
$1/64$	0.97	0.87	0.75	0.69	0.67	0.56	0.67	0.67	0.56	0.59
$1/32$	0.87	0.62	0.33	0.33	0.42	0.49	0.57	0.49	0.43	0.37
$1/20$	0.80	0.57	0.31	0.30	0.16	0.14	0.31	0.28	0.26	0.18
$1/16$	0.77	0.46	0.31	0.33	0.29	0.16	0.31	0.19	0.24	0.26
$\#$ \ t^∞	I_0	I_1	I_2	I_3	I_4	I_5	I_6	I_7	I_8	I_9
50	0.99	0.87	0.74	0.81	0.78	0.75	0.86	0.83	0.81	0.64
100	0.99	0.89	0.69	0.71	0.60	0.71	0.80	0.78	0.77	0.67
150	1.00	0.86	0.67	0.66	0.63	0.60	0.75	0.74	0.72	0.61
200	0.99	0.85	0.65	0.67	0.64	0.61	0.75	0.64	0.69	0.58

Averaged modified Kendall τ coefficients as a measure of correlation between the expected complexity ranks and the induced orders at $t^\infty \in \{0.1, 0.2, \ldots, 0.9\}$ are reported in Table 3.3. All of the coefficients are positive, with a minimum of 0.07 and a maximum of 0.96, implying that relative measurement can be used as a measurement of circularity. However, the coefficients decay with increase in t^∞ indicating that noise is not attenuated well.

Compared with the scores of entropy measurements on noisy squares, Table 2.1, it is seen that these scores are very low. For more accurate rankings, sums of relative entropy measurements over intervals of 0.1 of t^∞ are calculated. In doing so ten measurements are acquired for each control parameter. The averaged modified Kendall τ coefficients are reported in Table 3.4. In the table, I_0 denotes the interval $(0, 0.1]$, I_1 denotes $(0.1, 0.2]$, and so on. The correlations follow a similar trend as t^∞ increases, yet are improved, with a minimum of 0.14 and a maximum of 1.00.

Lastly, in Table 3.5, τ correlations of expected complexity ranks with sums of relative measurements over all t^∞ are presented. The correlations increase drastically, attaining a much better minimum of 0.73 and a maximum of 0.97.

All three tables show that it is easier to detect differences in grouped noise (as determined by nf) than to detect differences in scattered noise (as determined by $\#$): The average of Kendall τ correlations over all fixed-nfs is 0.41 for pointwise-t, 0.46 for

Table 3.5: Modified τ correlation coefficients averaged over fifty datasets of noisy discs between rankings by $\sum D^*(. \,||\, D_{64})$ in L^∞ and rankings by control parameters for each control parameter

nf	$1/64$	$1/32$	$1/20$	$1/16$
τ	0.97	0.83	0.73	0.77
$\#$	50	100	150	200
τ	0.91	0.97	0.99	0.97

regional-t, and 0.83 for all-t measurements; whereas over all fixed-$\#$s, it is 0.68 for pointwise-t, 0.75 for regional-t and 0.96 for total-t measurements.

CHAPTER 4

COMPARISON OF L^2 AND L^∞ MEASUREMENTS IN TERMS OF ENTROPY AND RELATIVE ENTROPY

A multi-scale method for measuring circularity can be acquired by using the Euclidean metric in constructing the field and the distance transform, instead of L^∞ metric. The field to be constructed is governed by

$$\left(\Delta - \frac{1}{\rho^2}\right) f_S^E = -1 \text{ subject to } f_S^E\Big|_{\partial S} = 0, \tag{4.1}$$

and has been proposed in [27].

The constructed field encodes a smooth transformation of the shape boundary to a more circular form as its level sets. This behavior is depicted in Fig. 4.1 for a circle and a square where level sets of circle remain circular, and level sets of square transform into a circle.

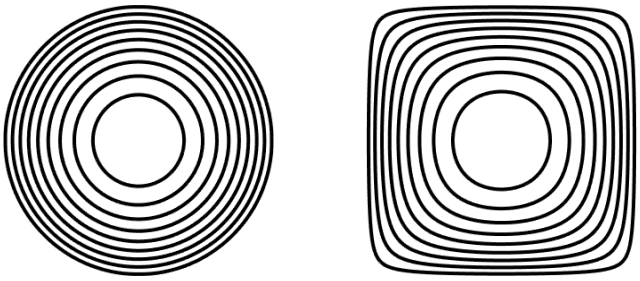

Figure 4.1: Level sets of constructed fields in L^2 for a square and a circle

In this chapter, entropy and relative entropy measurements in the Euclidean setting are compared with the proposed measurements.

4.1 Noisy Shapes

In this section, entropy measurements in L^2 are tested on the fifty datasets of noisy discs which are used in Subsec. 3.3.3 and exemplified by Fig. 3.11, and relative entropy measurements in L^2 are tested on the fifty datasets of noisy squares which are used in Subsec. 2.4.1 and exemplified by Fig. 2.10. The results are compared against the results of entropy and relative entropy measurements in L^∞.

4.1.1 Entropy measurements in L^2

For entropy measurements in L^2, adding noise to a disc corresponds to increasing the complexity of the shape. Hence, measurements are expected to yield orderings based on the amount of noise on the noisy discs. Modified Kendall τ correlation coefficients are computed to measure the similarity between the assigned complexity scores and the expected ones at $t^E \in \{0.1, 0.2, \ldots 0.9\}$. Results are presented in Table 4.1 as averages over fifty datasets, and in Table 4.2 as standard deviations of τ coefficients among fifty datasets.

Table 4.1: Averages of modified τ correlation coefficients of entropy measurements in L^2 over the fifty datasets of noisy discs

nf \ t^E	0.1	0.2	0.3	0.4	0.5	0.6	0.7	0.8	0.9
1/64	0.89	0.93	0.94	0.79	0.81	0.68	0.43	0.48	0.25
1/32	0.96	0.97	0.94	0.91	0.88	0.87	0.71	0.72	0.47
1/20	0.93	0.92	0.91	0.89	0.87	0.85	0.81	0.82	0.68
1/16	0.84	0.93	0.92	0.90	0.91	0.90	0.87	0.80	0.70
# \ t^E	0.1	0.2	0.3	0.4	0.5	0.6	0.7	0.8	0.9
50	1.00	1.00	0.99	0.97	0.99	0.93	0.90	0.88	0.67
100	1.00	1.00	1.00	1.00	0.99	0.96	0.95	0.92	0.85
150	0.99	0.99	0.99	1.00	1.00	0.99	0.97	0.95	0.89
200	1.00	1.00	1.00	1.00	1.00	0.99	1.00	0.98	0.95

Of the possible outcomes ranging from -1 to 1, all the entries of Table 4.1 are ≥ 0.25, with an average of 0.89 over all scales and control parameters. This indicates that the measure responds to noise in the expected way.

Table 4.2: Standard deviations of modified τ correlation coefficients of entropy measurements in L^2 over the fifty datasets of noisy discs

nf \ t^E	0.1	0.2	0.3	0.4	0.5	0.6	0.7	0.8	0.9
1/64	0.17	0.13	0.15	0.20	0.22	0.28	0.33	0.43	0.56
1/32	0.11	0.10	0.15	0.16	0.18	0.18	0.28	0.29	0.39
1/20	0.14	0.14	0.19	0.21	0.18	0.19	0.18	0.20	0.30
1/16	0.24	0.15	0.16	0.17	0.15	0.17	0.20	0.26	0.29
# \ t^E	0.1	0.2	0.3	0.4	0.5	0.6	0.7	0.8	0.9
50	0.00	0.00	0.05	0.09	0.07	0.13	0.15	0.16	0.28
100	0.00	0.00	0.00	0.00	0.05	0.11	0.12	0.14	0.24
150	0.05	0.05	0.05	0.00	0.00	0.05	0.09	0.12	0.18
200	0.00	0.00	0.00	0.00	0.00	0.05	0.00	0.08	0.12

τ coefficients decrease with increasing t^E, similar to the relative measurements in L^∞ and in contrast to the entropy measurements in L^∞. This decrease can be reasoned to be caused by the unattenuated boundary noise propagating through the field.

Table 4.3: Modified τ correlation coefficients averaged over fifty datasets of noisy discs between rankings by $\sum E_{t^E}$ and rankings by control parameters for each control parameter

nf	1/64	1/32	1/20	1/16
τ	0.89	0.91	0.93	0.93
#	50	100	150	200
τ	0.99	0.99	1.00	1.00

In Table 4.3, modified τ correlation coefficients between rankings by $\sum E_{t^E}$ for each control parameter and rankings by control parameters are presented. The coefficients for fixed nfs increases as nf increase. In both of the presented tables it is seen that detecting differences in number of noise addition is harder than detecting differences in noise factors.

We compare these results, first, with results of entropy measurements in L^∞ on noisy squares (*cf.* Tables 2.1 and 2.3), since both of the measurements are on the noisy balls of the respective metrics. The performances of measurements compete on small scales, especially on $t = 0.2$ and $t = 0.3$, with several dominances of L^2 over L^∞.

Nevertheless, when sums over control parameters are considered, results in L^∞ outperform those in L^2 at all scales.
It can be concluded from this comparison that entropy in L^∞ as a measurement of squareness is more reliable than entropy in L^2 is as a measurement of circularity.

Secondly, we compare the results of entropy measurements in L^2 with the results of relative entropy measurements with respect to a disc of radius 64 on noisy discs in L^∞ (*cf.* Tables 3.3, 3.4 and 3.5). Except for $nf = 1/64$ at $t \in \{0.7, 0.8, 0.9\}$, pointwise-t measurements in L^2 outperform pointwise-t measurements in L^∞, especially for $nf = 1/20$ and $nf = 1/16$ where τ correlation differences attain an average of 0.60 and a maximum of 0.85. The situation is similar with L^∞ regional-t measurements, despite the improvements. Comparing all-t measurements, it is seen that L^2 performs much better than relative L^∞ measurements on fixed-nf, except for $nf = 1/64$, and performs better on fixed-$\#$ scores, although not as drastically as it does for fixed-nf.

It is as expected that relative entropy in L^∞ to be outperformed by entropy in L^2 on noisy discs. This is because discs are the implicit references in L^2, whereas a specific disc is given as an explicit reference to relative measurements in L^∞.

4.1.2 Relative entropy measurements in L^2

Table 4.4: Averages of modified τ correlation coefficients of pointwise relative entropy measurements in L^2 with respect to a square over the fifty datasets of noisy squares

nf \ t^E	0.1	0.2	0.3	0.4	0.5	0.6	0.7	0.8	0.9
1/64	0.21	-0.13	-0.11	-0.52	-0.21	0.09	0.85	0.67	-0.05
1/32	0.91	0.90	0.86	0.86	0.68	0.73	0.62	0.85	0.49
1/20	0.92	0.91	0.89	0.87	0.73	0.79	0.75	0.72	0.70
1/16	0.86	0.83	0.83	0.81	0.69	0.77	0.77	0.73	0.71
$\#$ \ t^E	0.1	0.2	0.3	0.4	0.5	0.6	0.7	0.8	0.9
50	0.97	0.91	0.93	0.81	0.65	0.82	0.91	0.94	0.81
100	1.00	0.99	0.98	0.95	0.71	0.79	0.95	0.93	0.90
150	0.99	0.99	0.97	0.97	0.78	0.89	0.91	0.91	0.92
200	0.98	0.99	0.98	0.97	0.87	0.93	0.93	0.91	0.95

Now, we consider the relative entropy measurements in L^2 with respect to a square of

side length 128 on the noisy square datasets. It is assumed that the relative measurement corresponds to a measure of squareness. Therefore, it is expected to reflect the amount of noise in the assigned complexity scores.

First, consider the correlations of the induced orders with those determined by the control parameters at $t^E \in \{0.1, 0.2, \ldots, 0.9\}$. In Table 4.4, the averaged τ coefficients are given.

Except for the five negative ones, coefficients indicate positive correlation with the expected orders. The overall average of the given coefficients is 0.76 when the scores for $nf = 1/64$ are counted, and 0.84 when they are discounted. The negative scores indicate that L^2 relative entropy measurements are not able to tell the difference between added amount of noise when the added noise has a low shape radius. However, the negative scores with a minimum of -0.52 already signal an instability of the method.

Table 4.5: Averages of modified τ correlation coefficients of regional relative entropy measurements in L^2 with respect to a square over the fifty datasets of noisy squares

nf \ t^E	I_0	I_1	I_2	I_3	I_4	I_5	I_6	I_7	I_8	I_9
$1/64$	1.00	0.79	-0.07	-0.35	-0.25	0.43	0.83	0.85	0.85	0.41
$1/32$	0.97	0.91	0.79	0.88	0.77	0.87	0.79	0.69	0.85	0.69
$1/20$	0.94	0.92	0.90	0.92	0.89	0.89	0.83	0.77	0.83	0.68
$1/16$	0.87	0.87	0.85	0.87	0.81	0.79	0.75	0.77	0.75	0.65
$\#$ \ t^E	I_0	I_1	I_2	I_3	I_4	I_5	I_6	I_7	I_8	I_9
50	0.99	0.97	0.91	0.97	0.85	0.93	0.90	0.85	0.95	0.88
100	1.00	1.00	0.95	0.99	0.94	0.94	0.95	0.89	0.96	0.94
150	1.00	0.99	0.97	0.99	0.95	0.98	0.97	0.95	0.94	0.88
200	0.99	1.00	0.97	0.99	0.95	0.95	0.95	0.93	0.98	0.93

Table 4.5 reports the averaged τ coefficients of induced order by using regional complexity scores.

The coefficients are seen to increase significantly with a new minimum of -0.35 and three negative values. Clearly, the instability seen for $nf = 1/64$ is present despite using regional complexity scores. The overall average of the coefficients increase to 0.84. If the scores for $nf = 1/64$ are discarded this number increases to 0.89.

There is a downwards trend in τ coefficients of both the pointwise-t and regional-t measurements with increase in the scale parameter. Note that this trend, out of four considerations of noisy shapes, has not been seen only for entropy measurements in L^∞.

Table 4.6: Modified τ correlation coefficients averaged over fifty datasets of noisy squares between rankings by $\sum D^*(. \,||\, S_{128})$ in L^2 and rankings by control parameters for each control parameter

nf	$1/64$	$1/32$	$1/20$	$1/16$
τ	0.89	0.92	0.93	0.90
$\#$	50	100	150	200
τ	0.97	0.99	1.00	1.00

In Table 4.6 τ coefficients for measurements using all complexity scores are given. It is seen that the instable behavior for $nf = 1/64$ disappeared now. The τ coefficient for $nf = 1/64$ indicates that, in fact, relative L^2 measurements are able to account for noise of low shape radius, but it is able to do so only considering all the scales.

Comparing the pointwise-t results with the pointwise-t of L^∞ on squares (Table 2.1), it is seen that L^∞ is more successful at all t except at $t = 0.1$ for $nf = 1/32$ and $t = 0.2$ for $\# = 150$. Similar outranking of pointwise-t of L^∞ over regional-t results also holds. When the all-t results are considered, except for $\# = 200$ measurements, L^2 is outperformed by L^∞.
As in the case of relative L^∞ measurements and entropy measurements in L^2 on discs, it was expected that L^2 to be surpassed by L^∞ as the squares are the implicit references of L^∞.

We now turn to compare the performances of relative L^2 and L^∞ (*cf.* Tables 3.3, 3.4, and 3.5).
The overall mean of relative pointwise-t measurements in L^∞ is 0.59, and is worse than the mean of L^2, even when $nf = 1/64$ measurements are included. For the regional-t measurements the overall τ coefficient mean is 0.61 for L^∞, versus 0.84. The all-t measurements favor L^∞ in $nf = 1/64$ only.

Based on these, it can be said that L^2 method extends statistically better to a relative

measure than L^∞. However, it should be noted that L^2 depicts an instable behavior which is not overcome by regional-t measurements, that crosses off the multi-scale usability of the extended relative measure.

4.2 Appendages

The orders induced by entropy measurements in L^2 and L^∞ on two datasets composed of shapes of varying number of appendages are compared. One of the datasets is prepared by appending rectangular shapes to a square, and the other by appending circular appendages to a disc. Appendages are positioned either at the top, bottom, right or left of the main shape. Datasets are as presented in Fig. 3.1 and Fig. 3.5.

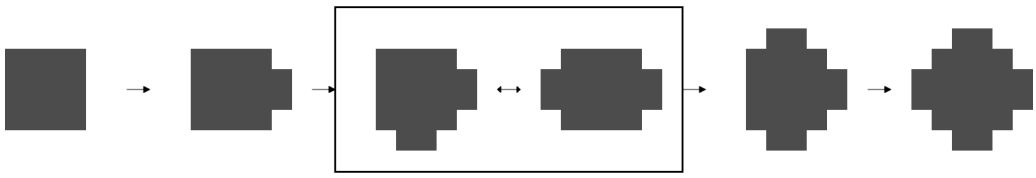

(a) $t^\infty \in \{0.01, 0.02, \ldots, 0.50\}$

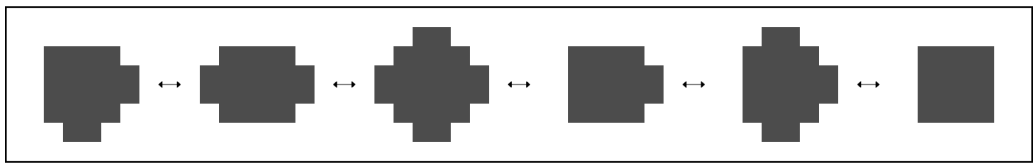

(b) $t^\infty \in \{0\} \cup \{0.51, 0.52, \ldots, 1\}$

Figure 4.2: Multi-scale orderings of squares of varying number of rectangular appendages in L^∞

The order induced on the rectangular set by f_S^∞ is displayed in Fig. 4.2. Until the cutoff level 0.5, the ordering is based on number of parts and is stable. Distinction between the two shapes with two appendages, S_{2a} and S_{2b} is not present, due to measurement's local behavior.

Fig. 4.3 displays the dominant orders induced on the circular set by f_S^E. The shown orders are not stable outside the indicated ranges of t^E. Plots of entropy measurements on the discs versus the scale parameter is displayed in Fig. 4.4

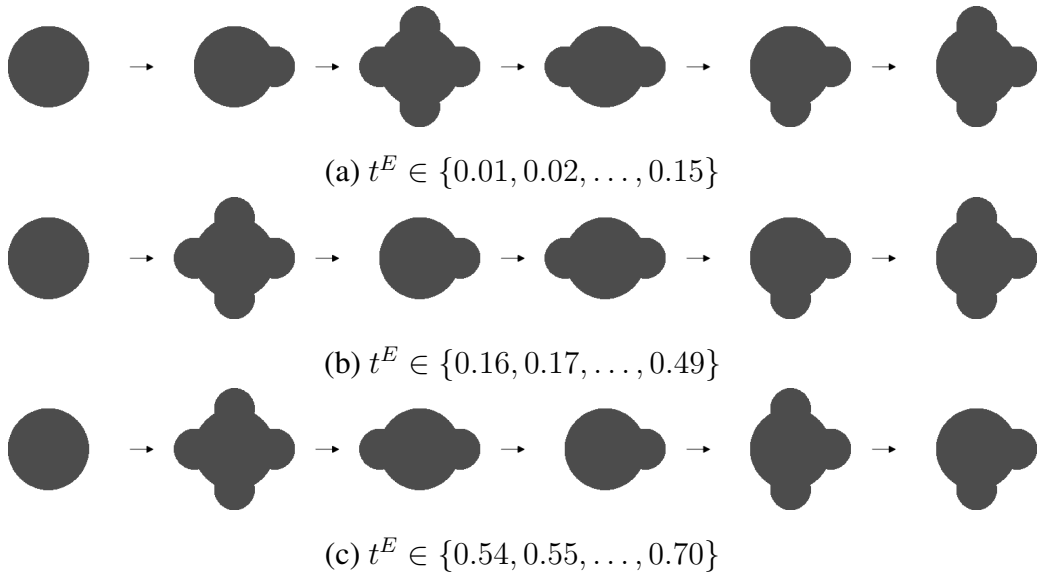

(a) $t^E \in \{0.01, 0.02, \ldots, 0.15\}$

(b) $t^E \in \{0.16, 0.17, \ldots, 0.49\}$

(c) $t^E \in \{0.54, 0.55, \ldots, 0.70\}$

Figure 4.3: Multi-scale orderings of discs of varying number of circular appendages in L^2

Near boundary measurements, shown in Fig. 4.3 (a), are based on number of parts except for D_4. Note that D_4 is the most symmetrical shape after D_0. It is also seen that D_{2a} is simpler than D_{2b} for all $t^E \in (0, 1)$ even though the order among other shapes change with changing scale. These indicate the presence of complexity reducing effect of symmetry across all scales.

As t^E increases, symmetry plays a more dominant role in on the complexity of the shapes. The change in the orderings of D_1 and D_{2a} attained at $t^E = 0.50$ is maintained stably for $t^E \in \{0.50, 0.51, \ldots, 0.99\}$.

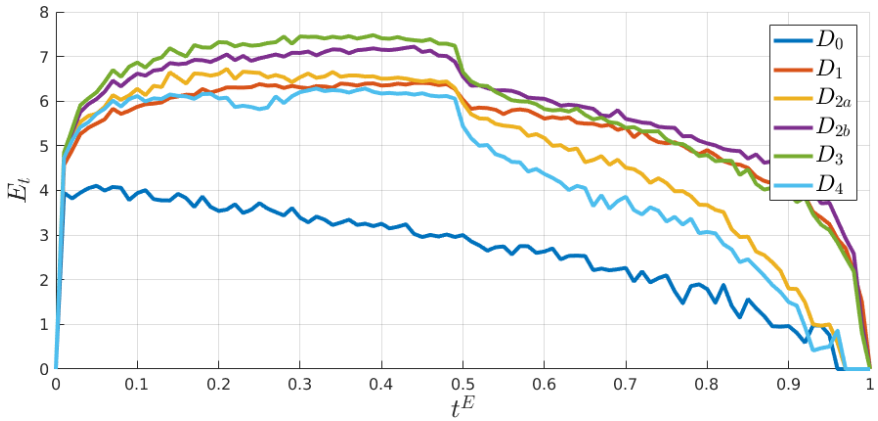

Figure 4.4: Entropy measurements in L^2 versus the scale parameter on discs with varying number of circular appendages

It is noteworthy to mention that for the dominant behavior of t^E in $\{0.70, 0.71, \ldots, 0.99\}$ shown in Fig. 4.3 (c) the order between D_1 and D_3, each with one symmetry axis, is sensitive.

Comparing the results of entropy measurements in L^∞ on squares with those of L^2 on discs, it is seen that measurements in L^∞ are more stable and predictable than the measurements in L^2. On the other hand, global properties such as symmetry is captured in L^2 with its impact varying with scale, whereas in L^∞ it is disregarded.

For a detailed analysis of relative entropy measurements on these two datasets in L^∞, we refer the reader to Subsec. 3.3.1.

4.3 Effects of Form and Size

Under this section we compare the effect of size on the complexity scores of shapes as acquired from entropy measurements in L^2 and L^∞, and from the inverse form factor given as $P^2/4\pi A$.

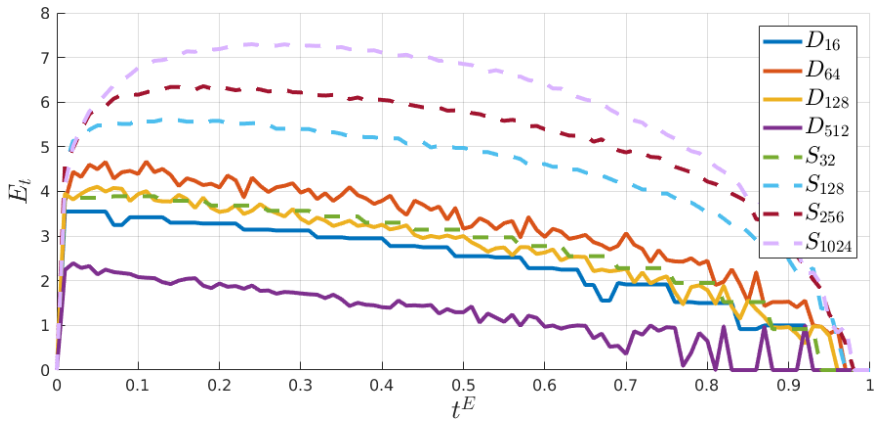

Figure 4.5: Entropy measurements in L^2 versus the scale parameter on discs of radii 16, 64, 128, 512, and squares of side lengths 32, 128, 256, 1024

Fig. 4.5 displays the complexity scores in L^2 versus the scale parameter t^E for discs of radii 16, 64, 128, 512, and squares of side lengths 32, 128, 256, 1024. The plots show that

1. discs do not attain zero-complexity,

2. it is possible for a square's complexity scores to be lower than a disc,

3. discs are inclined to attain lesser scores with increasing size,

4. squares attain higher scores with increasing size.

These results are in harmony with the continuous versus discrete setting discussions carried out in Sec. 1.2. In permitting the use of Euclidean metric, the theory treats digital shapes as approximations to the ideal forms. Hence, with more accurate approximations, a digital shape exhibits properties of the ideal form more strongly. As a result, as the accuracy of the approximation increase, squares are regarded more complex and discs simpler. This is not without exceptions though: a disc of radius 16 is observed to be simpler than discs of radii 64 and 128.

Since discs do not attain zero-complexity, it is possible for other shapes to attain lower complexity scores than a disc. This is readily shown in the plot 4.5 where a square of side length 32 attains a lower complexity than a disc of radius 64 almost at all $t^E \in (0, 1)$. This is a more serious problem than that of size-variance of the complexity scores, because the order among an approximation to the simplest shape, *i.e.* a disc, and an approximation to another shape, *i.e.* a square, is opposite to what is expected. That is, *when implemented, the theory contradicts its axioms*.

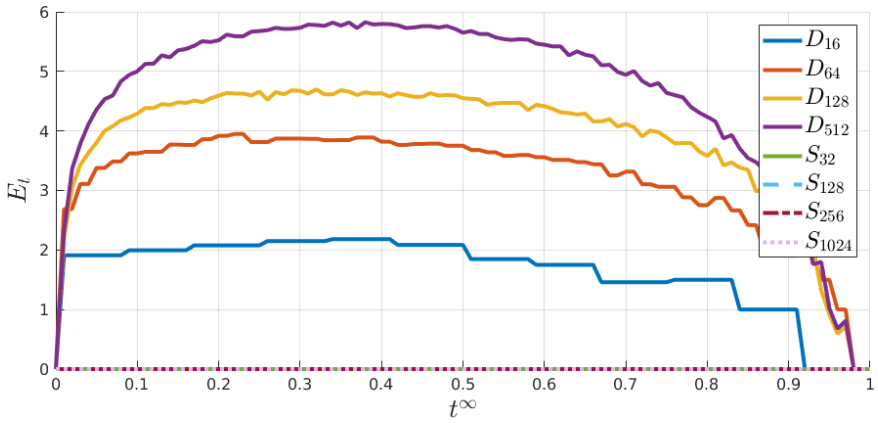

Figure 4.6: Entropy measurements in L^∞ versus the scale parameter on discs of radii 16, 64, 128, and 512; and squares of side lengths 32, 128, 256, and 1024

Now, consider the case of entropy measurements in L^∞, plots of which are displayed in Fig. 4.6. First, it is seen that, all of the squares attain zero-complexity for all

t^{∞}. Since this is the lowest permitted complexity score, it is not possible for another shape to attain a lower score than a square. It also means that the complexity scores for squares are scale independent. Second, complexities of the discs increase with increase in size almost at all $t^{\infty} \in (0, 1)$. This is because of the reducing presence of polygonal properties.

In Fig. 4.7, the resulting order using the inverse form factor is shown where the shapes are represented in log scale. It is seen that squares are found to be more complex than circles, and have increasing complexity scores with increasing size. Scores of discs, on the other hand, do not monotonically increase with increasing size: disc of radius 512 is less complex than disc of radius 128.
The inverse form factor is expected to attain its minimum for discs. However, the diamond attains the lowest score, as has been shown by Rosenfeld [11]. Moreover, since the accuracy of the approximation increases with increasing size, discs of larger radii should attain lower complexity, but the acquired results do not show an inclination towards such a trend.

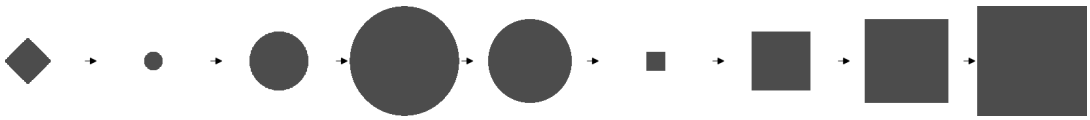

Figure 4.7: Order induced by the inverse form factor on a diamond of side length 48, discs of radii 16, 64, 128, 512, and squares of side lengths 32, 128, 256, 1024. The shapes are displayed in log scale.

CHAPTER 5

PARTIAL ORDER ON SHAPES

5.1 Motivation

Complexity is not well-defined. Since shapes are inherently infinite dimensional, there is no finite set of features that can account for all the variability of a shape [34]. Therefore, there is no canonical way of measuring shape complexity. As shown in Chapter 4 neither of the discussed methods is better than the others in all aspects.

It is, however, of practical concern to compare the shapes based on different complexity considerations. Under such circumstances, although a linear order cannot be established on the set of all shapes, it is possible to establish a partial order.
Partial order mainly differs from linear order by the presence of incomparable pairs of objects. From a constructed partial order, subsets of given shapes -*chains*- can be extracted on which a linear order is established.

5.2 Sample Results

In the following results, partial orders are constructed by using $(\leq)$ relation for each of the indicated measurements. The partial orders are represented with Hasse diagrams.

First, consider the L^2 and L^∞-entropy measurements on discs with circular appendages (see Fig. 4.3). If the results of L^2 at $t = 0.4$ and $t = 0.7$ are used, the resulting partial order is as shown in Fig. 5.1 (a). This partial order has four chains. It, for example, depicts that it is not possible to tell whether D_1 or D_{2a} is more complex, since the

used measurements do not agree on their order.

Adding the measurement at $t = 0.1$ to the set of used measurements, we obtain the partial order shown in Fig. 5.1 (b). The difference between the two is the incomparability of D_1 with D_4. Since the measurements of L^2 at lower scales dominantly correspond to boundary regularity, $E_{0.1}(D_1) \leq E_{0.1}(D_4)$.

It is also possible to use averages of the complexity scores. Partial order constructed using averaged L^∞-entropy scores at $t \in \{0.10, 0.11, \ldots, 0.25\}$ (low-t) and L^2-entropy at $t \in \{0.75, 0.76, \ldots, 0.90\}$ (high-t) is displayed in Fig. 5.1 (c). Since L^∞-entropy at low scales tends to measure complexity based on the number of appendages -except between D_4 and D_3 because D_4's boundary regularity outweighs its complexity due to the extra appendage- D_4 is incomparable with D_1, D_{2a} and D_{2b}.

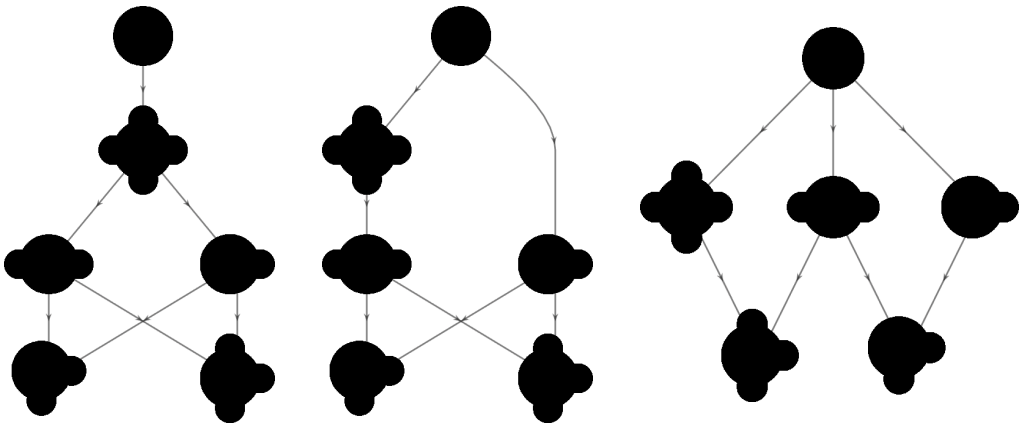

Figure 5.1: The obtained partial orders on discs with circular appendages using (a) L^2-entropy at $t = 0.4$ and $t = 0.7$, (b) L^2-entropy at $t = 0.1$, $t = 0.4$ and $t = 0.7$, (c) L^∞-entropy averaged at low-t and L^2-entropy averaged at high-t

Next, we turn to the measurements of L^∞-entropy on 'device3' of MPEG7 dataset. In Fig. 5.2 (a), measurements averaged at low-t and $t \in \{0, 0.01, \ldots, 1\}$ (all-t) are used. The first three shapes are ordered linearly based on the deformations of square. The third shape is followed by three others in different branches, each with a different kind of deformation: more concave, more oval, or more curved. All of them are considered less complex than the shapes of the cut group. Among the shapes of the cut group, the most complex is the one with curvy cuts.

Restricting ourselves to high-t, instead of all-t, in averaging the complexity scores,

we get the result displayed in Fig. 5.2 (b). At high scales, it is seen that the concave shape with sharp edges is not more complex than the third shape anymore. In fact, the shapes in the concave group are considered as practically squares at these scales (see: Fig. 3.9). The rest of the relationships are seen to be preserved.

The complete picture using the first set of measurements on 'device3' is given in Fig. 5.4.

As a last example, we construct a mixed set of shapes from MPEG7 dataset. In Fig. 5.3 (a) partial order on this set using L^{∞}-entropy measurements at low-t and high-t is displayed. The linear orders based on the respective measurements are given in Fig. 5.3 (b) and (c). At low-t, the boundary's rectangularity is considered, hence, faces attain lesser complexity scores than elephant and jar. However, at high-t, non-rectangular properties of faces are not attenuated as successfully as those of elephant and jar, both of which have a more rectangular body, especially elephant. Therefore, based on the used measurements elephant, faces and jar are incomparable with each other.
In both of the measurements, cup is considered as the least complex shape, and dog the most complex.

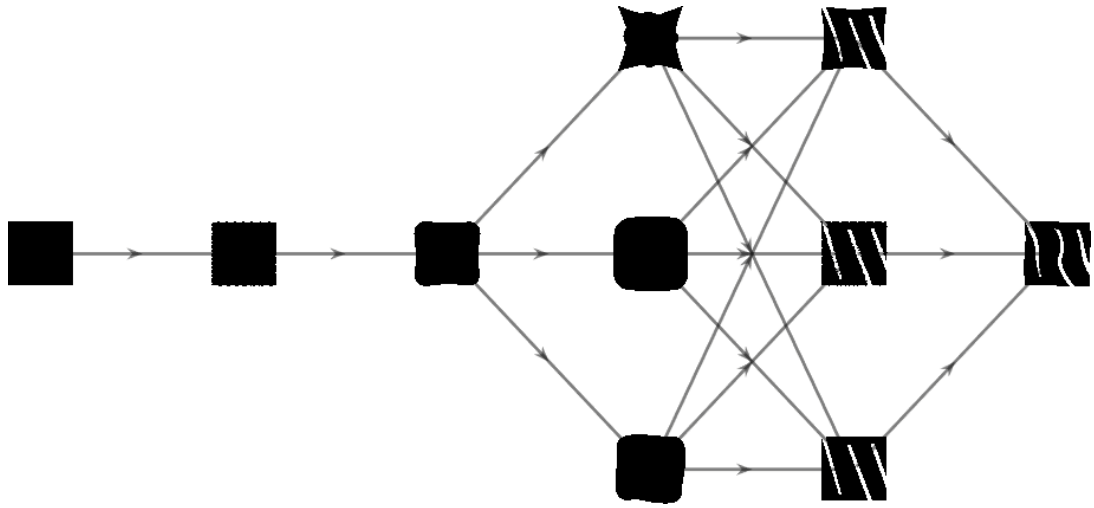

(a)

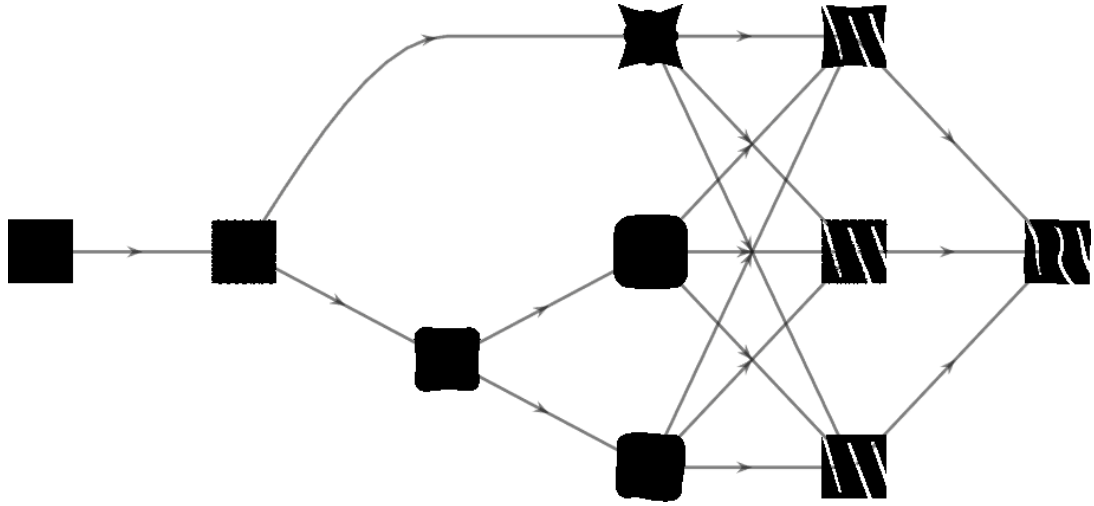

(b)

Figure 5.2: The obtained partial orders on shapes from 'device3' using L^∞-entropy measurements averaged at (a) low-t and all-t, (b) low-t and high-t

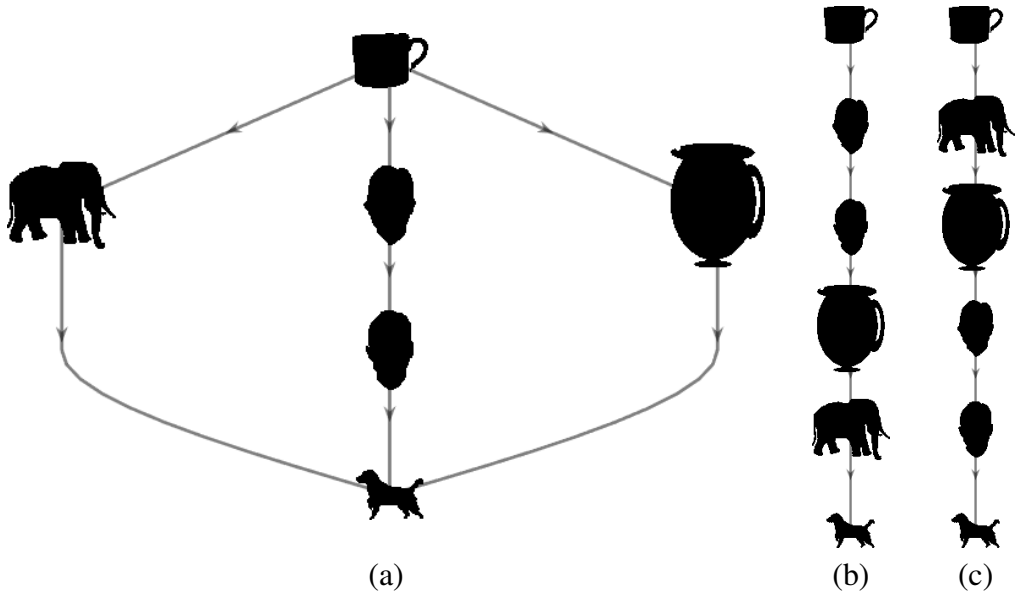

Figure 5.3: The obtained partial order (a) on a dataset consisting of a cup, jar, elephant, dog, and two human faces using L^∞-entropy measurements at low-t (b) and high-t (c)

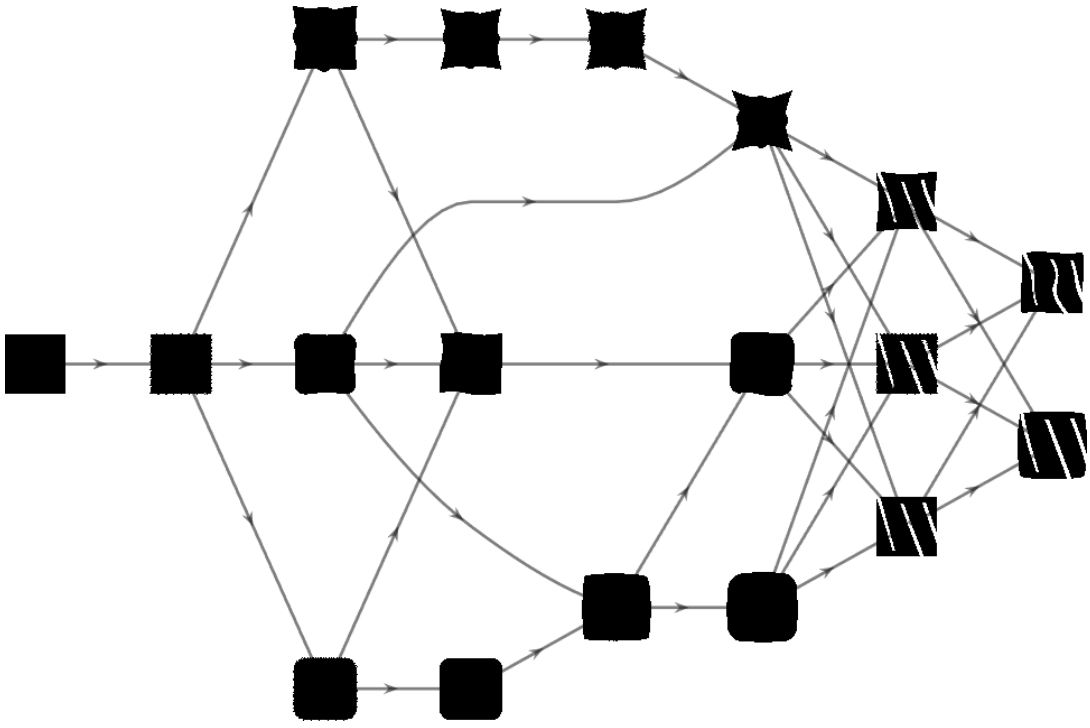

Figure 5.4: The partial order on all shapes -except for the duplicates- of 'device3' using L^∞-entropy measurements averaged at low-t and all-t

CHAPTER 6

ANALYTICAL SOLUTIONS OF SPE

In this chapter the connection between the screened Poisson equation in L^∞ and L^∞ distance transform is shown. Based on the analytical solutions for a square, a local measurement of rectangularity is proposed.

6.1 Analytical Solution of SPE in L^∞ for a Square

To acquire analytical solutions of SPE in L^∞ the following observations are made use of

1. in one dimension, partial derivatives in L^∞ are the same as in L^2, such as $\frac{\partial}{\partial x}$, $\frac{\partial^2}{\partial x^2}$,
2. value of f_S^∞ at a point is completely determined by its relation to the boundaries.

Note that, subjecting f_S^∞ to square-boundary condition in L^∞ necessitates the equivalence of values at points that are equidistant to the boundaries and the origin. To make this more clear, consider the points P_1 and P_2 as given in Fig. 6.1. Their distances to the nearest boundary and to the origin are the same, hence values of f_S^∞ are the same at P_1 and P_2. Furthermore, this holds for all points in R_1 whose y coordinates are the same, and identical arguments apply for points in R_2

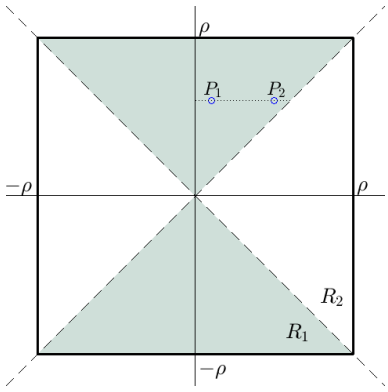

Figure 6.1: A square with sides aligned with grid axes

that share the same x coordinate. That is to say, $\partial f_S^\infty/\partial x = 0$ in R_1, and $\partial f_S^\infty/\partial y = 0$ in R_2. With these, in each of the regions R_1 and R_2, the problem of solving Eq. (2.2) reduces to a one-dimensional problem,

$$\begin{aligned} \frac{\partial^2 f_S^\infty}{\partial y^2} - \frac{1}{\rho^2} f_S^\infty &= -1, \quad \text{for } |y| \geq |x| \\ \frac{\partial^2 f_S^\infty}{\partial x^2} - \frac{1}{\rho^2} f_S^\infty &= -1, \quad \text{for } |y| < |x| \\ \text{subject to } f_S^\infty\Big|_{\partial S} &= 0. \end{aligned} \tag{6.1}$$

Solving for the homogeneous part in R_1, we get $f_{S,h}^\infty = A\exp\{y/\rho\} + B\exp\{-y/\rho\}$, and for inhomogeneous part $f_{S,p}^\infty = \rho^2$. Due to the symmetry of the boundary conditions, acquired solution is invariant under $y \mapsto -y$ changes. This dictates $A = B$. Applying the boundary condition we acquire

$$f_S^\infty\Big|_{R_1} = -\rho^2 \frac{e}{e^2+1}\Big(\exp\Big\{\frac{y}{\rho}\Big\} + \exp\Big\{-\frac{y}{\rho}\Big\}\Big) + \rho^2.$$

Following the same steps, solution in R_2 is acquired, and the joint solution is given in the closed form

$$f_S^\infty(x,y) = -\rho^2 \frac{e}{e^2+1}\Big(\exp\Big\{\frac{\max\{|x|,|y|\}}{\rho}\Big\} + \exp\Big\{-\frac{\max\{|x|,|y|\}}{\rho}\Big\}\Big) + \rho^2. \tag{6.2}$$

In this form the solution is not translation invariant. To satisfy translation invariancy, implicit reference to origin can be removed by reformulating the solution in terms of the L^∞ (chessboard) distance transform. Note that $\max\{|x|,|y|\} = \|\vec{p}\|_\infty$ where $\vec{p} = (x,y)$. Thus, we can rewrite Eq. (6.2) as

$$f_S^\infty\Big|_S = -\rho^2 \frac{e}{e^2+1}\Big(\exp\{t'^\infty\} + \exp\{-t'^\infty\}\Big) + \rho^2. \tag{6.3}$$

where $t'^\infty = 1 - t^\infty$. Since $f_S^\infty = f_S^\infty(t^\infty)$ for a square, it is now straightforward to see that the level sets of f_S^∞ and t^∞ agrees. Moreover, Eq. (6.3) is also the solution for cubes of arbitrary dimensions, *i.e.* n-cubes. The respective solutions for n-cubes can be acquired by following the same construction given above.

6.2 A Local Measurement of Rectangularity

In Fig. 6.2, the difference between the analytical solution and numerical solution for a square of side length 256 is displayed. The maximum absolute difference, $\max(|f_{analytical} - f_{numerical}|)$ is 0.00091. The error rate of the numerically acquired field is

$$\frac{\int |f_{analytical} - f_{numerical}|}{\int f_{analytical}} \approx 0.00102.$$

This difference is due to the calculation of the field to a first order approximation.

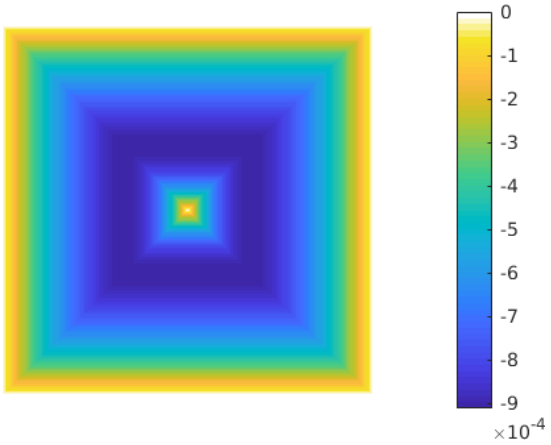

Figure 6.2: The difference between the analytical and numerical solutions for a square of side length 256

Similar to the circularity measurement proposed in [20], the discrepancy between the analytical and numerical solutions can be used as a local measurement of rectangularity. The differences between the numerically acquired solution and the analytical solution given by Eq. (6.3) is used as the rectangular-discrepancy field. This amounts to calculating error for the SPE field due to assuming that a given point is located inside a rectangle whose size is determined by the shape's radius and location is determined by the given point's distance to the closest boundary.

The rectangular-discrepancy field for squares with two appendages are shown in Fig. 6.3. In the figure, edges of the shapes are added manually.
Due to the significant change in the maximum difference value (~ 0.0009 against ~ 0.25), the error due to numerical imprecision is not visible in this figure. Areas of disagreement mark the appendages and their region of effect.

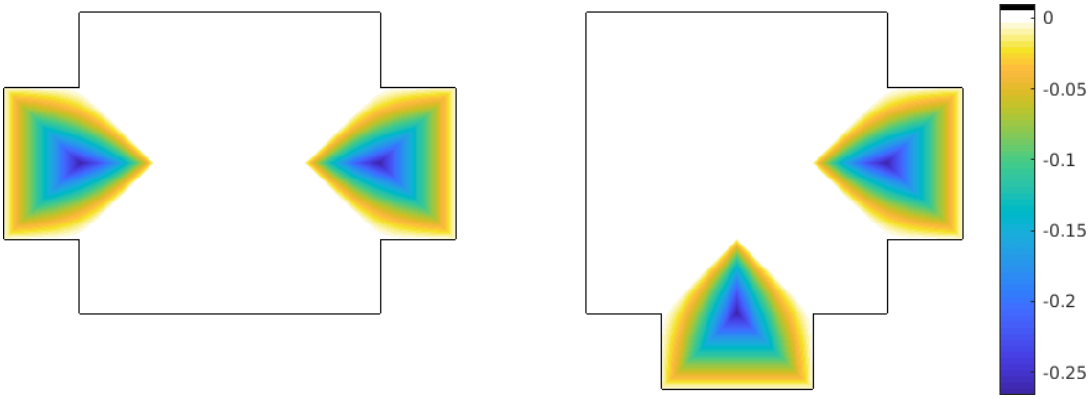

Figure 6.3: The rectangular-discrepancy field for squares with two appendages. The boundaries are added manually.

As a more complex example, the discrepancy field for an elephant is shown in Fig. 6.4. It is seen that the areas of highest disagreement are the legs and trunk, followed by the tail, ivories and head.

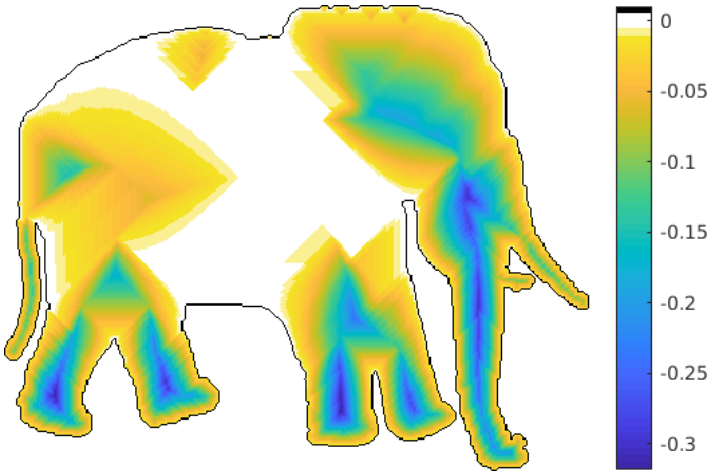

Figure 6.4: The rectangular-discrepancy field for an elephant silhouette. The boundaries are added manually.

CHAPTER 7

SUMMARY AND CONCLUSIONS

In this thesis, computational shape complexity is investigated. The investigation is guided by the discrete nature of digital computers and the relative nature of complexity. The aim of the chapters and the flow between them is as follows: By addressing the discrete nature of digital computers, it is reasoned that squares are the simplest shapes. In this vein, a measure for quantifying shape complexity is developed in Chapter 2. By addressing the relative nature of complexity, this method is extended to a relative measure of complexity in Chapter 3. The needed comparisons are made in Chapter 4 between the developed methods and their Euclidean equivalents. It is shown that neither of the methods are canonical for considerations of complexity, *i.e.* their performances change with differing views of complexity. This leads to the idea of constructing partial orders, which is investigated in Chapter 5 in the light of the findings of prior chapters. Chapter 6 aims to prove a claim made in Chapter 2 and does so by giving a novel analytical solution to the field proposed there.

In Chapter 2 a multi-scale shape complexity measure is proposed. The proposed measure relies on the realizability of squares in the digital space, and the fact that they are the circles in L^∞. Based on this a differential equation governed by infinity Laplacian is used to embed level sets inside shapes. The embedded level sets are *smoothed* versions of level sets of L^∞ distance transform. By restricting the field to the level sets of the distance transform, and partitioning these values into bins a distribution is acquired. The entropy of this distribution is then gives the complexity of the shape at a scale, where level sets of the normalized distance transform serves as a natural scale parameter. Since the level sets of proposed field and the distance transform agree for a square, the squares emerge as the simplest shape. Although the

measure is formulated in continuous space, its restriction to digital space has desirable properties which are listed below.

- Up to first order approximation, the field is governed by morphological operators (Subsec. 2.2.1). Hence, it inherits their properties, notably, the computational robustness.
- Level sets of the proposed field becomes locally flat (Fig. 2.1). Therefore, simplicity is in the favor of shapes whose boundaries aligned with the grid axes.
- A cutoff level emerges for rectangular appendages (Figures 2.3 and 2.4) and for apertures (Fig. 2.9) beyond which they no effect on the field.
- Orders on shapes with changing number, width and location of rectangular appendages are like the dictionary order (Fig. 2.7). This shows that discrimination between such physical variations is intrinsically encoded in the proposed measure.
- Perceptually more complex objects such as bats with regards to house plans are also considered as more complex by the measure (Fig. 2.9).
- Orders on shapes are very robust under additive noise (Subsec. 2.4.1).
- The proposed field and measure can be generalized to n-dimensions (Subsec. 2.4.2).

Notice that neither of these properties are especially addressed, rather *they emerged from addressing the computational aspects of shapes*.

In Chapter 3 the method is extended to a relative one to address the relative nature of shape complexity. This is done by calculating Kullback-Leibler (KL) divergence (with an additional penalty term) between the acquired distributions from a shape and the reference shape at the same scale. The remarks from this chapter are listed below.

- The modified divergence measure $D^*(P \,||\, Q)$ agrees with KL divergence whenever the support of P is a subset of the support of Q. In other words, the mod-

ified divergence extends KL divergence, in that, whenever KL divergence is applicable, it is used.

– Relative measurements are able to induce order on shapes of varying number of identical appendages. Given the shape with least number of appendages, the order is characterized by increasing number of appendages (Figures 3.2 and 3.6); and given the shape with highest number of appendages the order is characterized by decreasing number of appendages (Figures 3.3 and 3.7).

– For relative measurements, adding an appendage is a similar process than removing one (Figures 3.4 and 3.8.

– Range of complexity changes significantly with the chosen reference shape. This is reasoned to be caused by the reference shape's support's range.

– Complexity trends of shapes carry significant information that is available to manipulate by tools other than KL-divergence. For example, the location of the peaks indicate the reason for complexity; and so does the location of last nonzero (Fig. 3.9).

– The trends suggest clusters in accordance with human vision.

– Relative measurements are able to account for the amount of noise present on the noisy versions of the given reference shape (Tables 3.3, 3.4 and 3.5). However, they are not as reliable as the non-relative measure.

– The accountability of relative measurements in handling noise increases significantly when regional complexity scores are used in estimating the order on the shapes.

In Chapter 4 comparisons between the developed methods, and their Euclidean equivalents are carried out on noisy shapes, shapes with appendages and shapes with different forms and sizes. The behavior of the field constructed in L^2 is also given. Results of the comparisons are listed below.

– The performance of L^2-entropy on noisy discs is worse than the performance of L^∞-entropy on noisy squares (Tables 4.1, 4.3, 2.1 and 2.3).

– It is observed that detecting differences in applications of noise adding algorithm (*i.e.*, changes in $\#$) is harder than detecting differences in the noise factor for the L^2-entropy (Tables 4.1 and 4.3).

– L^2-entropy yields worse results at higher scales, which indicates that noise propagates through the constructed field (Table 4.1).

– L^2-relative entropy measurements on squares depict instable behavior with negative Kendall τ coefficients (Tables 4.4 and 4.5). However, they perform better than L^∞-relative entropy measurements on discs overall.

– Both of the tested relative measurements perform worse than the entropy measurements. This is expected since the reference shape is given explicitly in relative entropy measurements, and implicitly in entropy measurements. Nonetheless, relative measurements do have their use cases: when the reference shape is not the minimizing shape of some metric for which the discretization of the Laplacian is known.

– L^2-entropy measurements yield instable orders across the scale parameter. However, they grasp global properties such as symmetry in higher scales (Fig. 4.3).

– L^2-entropy measurements showed that (Fig. 4.5)

  ◦ discs do not attain zero-complexity,

  ◦ it is possible for a square's complexity scores to be lower than a disc,

  ◦ discs are inclined to attain lesser scores with increasing size,

  ◦ squares attain higher scores with increasing size.

– For both of the tested methods (L^2 and form factor) that assumed circles to be the simplest shapes, other shapes were found simpler (Figures 4.5 and 4.7).

– L^∞-entropy evaluated the complexity of squares as 0 regardless of their size, and ordered discs based on their sizes. This is due to the reducing presence of polygonal properties with increasing size.

In Chapter 5 partial orders on discs with appendages, shapes from 'device3', and a mixed dataset consisting of silhouettes of a cup, jar, elephant, dog, and two human

faces are presented. It is emphasized that *the order between the shapes is dynamic* and depends on how they are perceived.

In Chapter 6 analytical solution of SPE in L^∞ for a square is given. The solution supports the claim that the proposed field is a well-behaving chessboard distance transform.
Using the analytical solution for a square, a local measurement of rectangularity is established. Results are shown for squares with two appendages and an elephant silhouette. The resulting discrepancy field suggests that the local measurement can be used for image segmentation.

REFERENCES

[1] C. E. Shannon, "A mathematical theory of communication," *Bell System Technical Journal*, vol. 27, no. 3, pp. 379–423, 1948.

[2] R. Lopez-Ruiz, H. L. Mancini, and X. Calbet, "A statistical measure of complexity," *Physics Letters A*, vol. 209, no. 5-6, pp. 321–326, 1995.

[3] A. N. Kolmogorov, "Three approaches to the quantitative definition of information," *Problems of Information Transmission*, vol. 1, no. 1, pp. 1–7, 1965.

[4] N. Ritter and J. Cooper, "New resolution independent measures of circularity," *Journal of Mathematical Imaging and Vision*, vol. 35, no. 2, pp. 117–127, 2009.

[5] V. Blåsjö, "The isoperimetric problem," *The American Mathematical Monthly*, vol. 112, no. 6, pp. 526–566, 2005.

[6] F. Attneave, "Physical determinants of the judged complexity of shapes.," *Journal of Experimental Psychology*, vol. 53, no. 4, p. 221, 1957.

[7] H. Thomas, "Spatial models and multidimensional scaling of random shapes," *The American Journal of Psychology*, vol. 81, no. 4, pp. 551–558, 1968.

[8] M. D. Arnoult, "Prediction of perceptual responses from structural characteristics of the stimulus," *Perceptual and Motor Skills*, vol. 11, no. 3, pp. 261–268, 1960.

[9] A. Gartus and H. Leder, "Predicting perceived visual complexity of abstract patterns using computational measures: The influence of mirror symmetry on complexity perception," *PloS one*, vol. 12, no. 11, 2017.

[10] D. C. Donderi, "Visual complexity: a review.," *Psychological Bulletin*, vol. 132, no. 1, p. 73, 2006.

[11] A. Rosenfeld, "Compact figures in digital pictures," *IEEE Transactions on Systems, Man, and Cybernetics*, no. 2, pp. 221–223, 1974.

[12] P.-E. Danielsson, "A new shape factor," *Computer Graphics and Image Processing*, vol. 7, no. 2, pp. 292–299, 1978.

[13] R. S. Montero and E. Bribiesca, "State of the art of compactness and circularity measures," in *International mathematical forum*, vol. 4, pp. 1305–1335, 2009.

[14] L. Dorst, A. W. Smeulders, *et al.*, "Length estimators for digitized contours.," *Computer Vision, Graphics, and Image Processing*, vol. 40, no. 3, pp. 311–333, 1987.

[15] P. L. Rosin, "Measuring shape: ellipticity, rectangularity, and triangularity," *Machine Vision and Applications*, vol. 14, no. 3, pp. 172–184, 2003.

[16] P. Maragos, "Pattern spectrum and multiscale shape representation," *IEEE Transactions on Pattern Analysis and Machine Intelligence*, vol. 11, no. 7, pp. 701–716, 1989.

[17] D. L. Page, A. F. Koschan, S. R. Sukumar, B. Roui-Abidi, and M. A. Abidi, "Shape analysis algorithm based on information theory," in *International Conference on Image Processing, 2003.*, vol. 1, pp. 229–232, 2003.

[18] Y. Chen and H. Sundaram, "Estimating complexity of 2d shapes," in *2005 IEEE 7th Workshop on Multimedia Signal Processing*, pp. 1–4, 2005.

[19] A. Genctav and S. Tari, "A product shape congruity measure via entropy in shape scale space," *arXiv preprint arXiv:1709.03086*, 2017.

[20] A. Genctav and S. Tari, "Discrepancy: local/global shape characterization with a roundness bias," *Journal of Mathematical Imaging and Vision*, vol. 61, no. 1, pp. 160–171, 2019.

[21] P. L. Rosin, "Measuring rectangularity," *Machine Vision and Applications*, vol. 11, no. 4, pp. 191–196, 1999.

[22] P. L. Rosin and J. Žunić, "Measuring squareness and orientation of shapes," *Journal of Mathematical Imaging and Vision*, vol. 39, no. 1, pp. 13–27, 2011.

[23] J. Žunić and P. L. Rosin, "Measuring shapes with desired convex polygons," *IEEE Transactions on Pattern Analysis and Machine Intelligence*, 2019.

[24] D. J. Weintraub, "Rectangle discriminability: Perceptual relativity and the law of pragnanz.," *Journal of Experimental Psychology*, vol. 88, no. 1, p. 1, 1971.

[25] D. Moser, H. G. Zechmeister, C. Plutzar, N. Sauberer, T. Wrbka, and G. Grabherr, "Landscape patch shape complexity as an effective measure for plant species richness in rural landscapes," *Landscape Ecology*, vol. 17, no. 7, pp. 657–669, 2002.

[26] J. Hu, A. Razdan, J. C. Femiani, M. Cui, and P. Wonka, "Road network extraction and intersection detection from aerial images by tracking road footprints," *IEEE Transactions on Geoscience and Remote Sensing*, vol. 45, no. 12, pp. 4144–4157, 2007.

[27] Z. S. G. Tari, J. Shah, and H. Pien, "A computationally efficient shape analysis via level sets," in *Proceedings of the Workshop on Mathematical Methods in Biomedical Image Analysis*, pp. 234–243, IEEE, 1996.

[28] G. Aronsson, "On the partial differential equation $u_x^2 u_{xx} + 2u_x u_y u_{xy} + u_y^2 u_{yy} = 0$," *Arkiv för Matematik*, vol. 7, no. 5, pp. 395–425, 1968.

[29] A. Oberman, "A convergent difference scheme for the infinity laplacian: construction of absolutely minimizing lipschitz extensions," *Mathematics of Computation*, vol. 74, no. 251, pp. 1217–1230, 2005.

[30] P. Maragos, "Differential morphology and image processing," *IEEE Transactions on Image Processing*, vol. 5, no. 6, pp. 922–937, 1996.

[31] R. W. Brockett and P. Maragos, "Evolution equations for continuous-scale morphology," in *[Proceedings] ICASSP-92: 1992 IEEE International Conference on Acoustics, Speech, and Signal Processing*, vol. 3, pp. 125–128, IEEE, 1992.

[32] J. A. Cuesta and C. Matrán, "Conditional bounds and best l^∞-approximations in probability spaces," *Journal of Approximation Theory*, vol. 56, no. 1, pp. 1–12, 1989.

[33] S. Kullback, *Information Theory and Statistics*. Courier Corporation, 1997.

[34] E. Sharon and D. Mumford, "2d-shape analysis using conformal mapping," *International Journal of Computer Vision*, vol. 70, no. 1, pp. 55–75, 2006.